Eur. Phys. J. Spec. Top. (2023) 232:1813–1833
https://doi.org/10.1140/epjs/s11734-023-00803-x

THE EUROPEAN PHYSICAL JOURNAL SPECIAL TOPICS

Review

Introduction to topological defects: from liquid crystals to particle physics

Sébastien Fumeron[a] and Bertrand Berche[b]

Laboratoire de Physique et Chimie Théoriques, Université de Lorraine, CNRS, Nancy, France

Received 31 August 2022 / Accepted 24 February 2023 / Published online 13 April 2023

Abstract Liquid crystals are assemblies of rod-like molecules which self-organize to form mesophases, in between ordinary liquids and anisotropic crystals. At each point, the molecules collectively orient themselves along a privileged direction, which locally defines an orientational order. Sometimes, this order is broken, and singularities appear in the form of topological defects. This tutorial article is dedicated to the geometry, topology, and physics of these defects. We introduce the main models used to describe the nematic phase and discuss the isotropic–nematic phase transition. Then, we present the different families of defects in nematics and examine some of their physical outcomes. Finally, we show that topological defects are universal patterns of nature, appearing not only in soft matter, but also in biology, cosmology, geology, and even particle physics.

1 Introduction

Sometimes the deepest physics occurs just before our eyes, without really being noticed for decades except as a meaningless and minor accident of nature. Open your hand and look closer at your fingerprints: most of the folds extend regularly, but sometimes, at the tip of the fingers or in the palm of the hand, they engage in strange circumvolutions serving no purpose, apart from fortunetellers and forensics. In fact, these seemingly innocent-looking patterns are some of the most fascinating objects in nature: topological defects. They are at the crossroads of mathematics (topology, geometry) and physics (statistical physics but also cosmology or mechanical engineering for example) [1].

The present tutorial is primarily intended for students and researchers from the condensed matter physics community, but it may also be a useful resource to any theoretical physicist interested in the many bridges connecting different areas of physics. It is aimed as a self-contained introduction to topological defects in physics, and it is split into three parts. The first section is designed as a primer on nematic liquid crystals. After noting some historical milestones, we review the main models that can be used to describe the nematic order (Frank–Oseen, Maier–Saupe, Landau–de Gennes, and Lebwohl–Lasher). Then, we discuss the topology of the isotropic—nematic phase transition in connection with the formation of topological defects.

In the second section, we present the basics of nematoelasticity and establish a classification of the different linear defects that can be observed in liquid crystals. The geometric description of defect lines in terms of Riemann manifolds is introduced, and the general metric of a disclination is derived from a variational principle. Some outcomes on transport phenomena are discussed, in particular the possibility to generate Berry phases.

The last section is a survey of different problems where the same linear defects occurring in liquid crystals have been recognized as the key factor. A particular emphasis will be put on biology, as tissues display an orientational order similar to the nematic order. We will see that defects play a pivotal role in morphogenesis and oncology. Particular attention will also be paid to cosmology, since singularities called cosmic strings seem to be in perfect correspondence (formation, geometry, dynamics) with the defect lines in nematics.

2 A crash course on liquid crystals

2.1 A story of carrots and sticks

Liquid crystals have invaded our everyday lives, from flat screens (liquid crystal displays or LCDs) to anti-counterfeiting technologies used in banknotes. The tale

[a] e-mail: sebastien.fumeron@univ-lorraine.fr (corresponding author)
[b] e-mail: bertrand.berche@univ-lorraine.fr

Fig. 1 Patterns in human fingerprints. The values $m = \pm 1/2$ indicated there are explained later in this article

of liquid crystals is a fascinating story (for comprehensive accounts see [2–6]), and as is often the case in the history of science, their discovery started from a considerably less utilitarian premise. The first observations of what is now understood as liquid crystalline behavior were reported on myelin, a lipidic substance surrounding nerve cores, by Rudolf Virchow in 1850 (the discoverer of white blood cells) and Carl von Mettenheimer (the personal physicist of Arthur Schopenhauer) in 1857. In 1888, an Austrian botanist, Friedrich Reinitzer, was investigating the role played by cholesterol compounds contained in carrots. He successfully extracted crystals of cholesteryl benzoate and started to put them through a series of experimental tests. One of them consisted in measuring their melting point, which was expected to be precisely and uniquely defined for pure crystals. Reinitzer observed a melting point at about 145.5° C, at which cholesteryl benzoate crystals turn into a milky liquid that displays both double refraction and optical activity, properties usually assumed to belong to solid crystals. But against all odds, he found a second point at 178.5° C, at which the turbid liquid becomes transparent [7].

The perspective of a pure chemical compound having two melting points really bothered Reinitzer, and on March 14 of the same year, he wrote a letter to ask a renowned crystallographer, Otto Lehmann, about his observations. At that time, Lehmann had a position at the technical high school in Aachen and he was famous for inventing the "crystallization microscope," an apparatus coupling a regular optical microscope with two crossed optical polarizers and a thermal deck. From samples provided by Reinitzer, Lehmann found that the turbid phase can indeed flow like a liquid but behaved optically like an anisotropic crystal [2]. He eventually launched an extensive program of experiments to discover other substances behaving like the turbid liquid. In 1904, Lehmann summed up his discoveries in a monograph entitled "Flüssige Krystalle" ("flowing crystals") [8], a term which later evolved into "liquid crystals."

An important breakthrough was performed in 1907 by chemist Daniel Vorländer, from the University of Halle. Vorländer realized that the optical and mechanical properties of the milky liquid originate from the elongated structure of the molecules comprising it [5]. He used his knowledge of molecular structure to become the first chemist to systematically synthesize liquid crystals (more than 2000 compounds were designed in his group). Despite these advances, liquid crystals were still not recognized as a noble research topic, partly because of the vivid opposition of leading chemists such as Gustav Tammann, Walther Nernst, Georg Quincke, and Tadeusz Rotarski, partly because of Lehmann's personality, a mix of priggishness and mysticism (mostly the result of his bounds with Ernst Haeckel).

The gravity center of liquid crystal research shifted from Germany to France after a set of lectures given by Lehmann at the faculty of Sorbonne in 1909 [4, 5]. Lehmann personally invited the mineralogist Frédédric Wallerant and his assistant Charles Mauguin, both from Sorbonne, but his works also raised the interest of Paul Gaubert, then heading the mineralogy laboratory of the Museum of Natural History in Paris, and that of two geologists from the Ecole des Mines in Saint-Etienne, George Friedel and his assistant François Grandjean. In 1922, Friedel made the most significant landmark discovery in the development of liquid crystal. Being assemblies of microscopic sticks, liquid crystals display physical properties that prevent them from being either isotropic fluids or crystalline solids. In a seminal paper [9], Friedel argued that liquid crystals were new intermediate phases of matter, or mesophases, and he classified these mesophases into three main families, known as nematic, smectic, and cholesteric phases.

Nowadays, these classifications have been enriched with many newcomers such as the elusive blue phases I, II, and III [10, 11], the columnar phases [12], the hexatic phases, originally foreseen by John Kosterlitz and David Thouless [12–14], and the cubatic phases [15]. It is now understood that these different mesophases are intimately related to the chemical structure of the mesogenic molecules comprising them. Amphiphilic molecules have their head and tail displaying opposite chemical affinities. When dissolved in water, the hydrophobic and the hydrophilic groups organize into membranes and micelles, which give rise to lyotropic mesophases (blue phases, cubic phases, hexagonal phases, or lamellar phases) driven by the molecular concentration. Nematogenic molecules are partially rigid, generally because of phenyl groups, and bear electric dipoles (a carbonitrile group for 5CB, Schiff's base for *N*-(4-methoxybenzylidene)-4-butylaniline [MBBA], etc.). They form temperature-driven or thermotropic mesophases where the Van der Waals interactions are of the order of the thermal agitation. There also exist amphotropic mesophase, which share both lyotropic and thermotropic properties.

2.2 Mathematical theories of the nematic phase

For thermotropic nematics, on which we will focus hereafter, the molecules of liquid crystals may be described by long, neutral rigid rods, which interact through electrostatic dipolar or higher-order multipolar interactions. Maximization of entropy at high temperatures leads to a disordered phase in which all the molecule orientations are equally probable, independently of the directions taken by neighboring molecules: this is the isotropic phase. At low temperatures, a privileged orientation becomes favorable to minimize the molecular interactions, and various ordered structures may emerge spontaneously [16, 17]. The nematic phase is thus a compromise between the attractive van der Waals interactions that align rigid cores on average along the same direction (anisotropy) and the thermal agitation of the aliphatic chains increasing the mean steric hindrance (fluidity).

When order occurs along one space dimension only, the system is said to be uniaxial. The preferential direction which emerges after averaging at the mesoscopic scales, defines a unit vector, $\vec{n}$, called the director field. The dipole–dipole interactions tend to align molecules head-to-tail, which was confirmed by X-ray diffraction in the cyanobiphenyls 5CB and 7CB [18]. Therefore, there is statistically no preferential arrangement of the molecule ends and $\vec{n} \equiv -\vec{n}$: this is called Z_2 symmetry. This dictates that the order parameter should be a function of $\cos^2\theta$, with θ the angle between a molecule and the director field, rather than of $\cos\theta$ as in ordinary magnets (Zeeman interaction). Ideally, the order parameter should be normalized and mark a clear difference between a narrow distribution about $\pm\vec{n}$ and a random one. A choice fulfilling all these criteria is the scalar parameter proposed by Tsvetkov [19]:

$$S = \langle P_2(\cos\theta)\rangle = \frac{1}{2}\left(3\langle\cos^2\theta\rangle - 1\right) \tag{1}$$

where $P_2(x)$ is the second-order Legendre polynomial[1] and $\langle . \rangle$ is the ensemble average performed over all molecules in the nematic.

The simplest way to describe the nematic phase is to rely on a mean-field theory, for which the microscopic details are blurred into a larger-scale continuous field. The main continuum theories describing nematic liquid crystals are the Oseen–Frank theory, the Maier–Saupe theory, and the Landau–de Gennes theory.

The Frank–Oseen model is based on minimizing the free elastic energy [20, 21]: it is probably the simplest one to get the essential features of the nematic phase, even it fails at describing accurately the isotropic–nematic phase transition or the internal structure of defects (they have infinite energy). We will present it in more details in Sect. 3 to determine the outer structures of disclinations.

[1] Note that the choice of the second Legendre polynomial here implicitly assumes three-component $\vec{n}$ vectors. For two-component vectors, a different choice is needed [74].

In the Maier–Saupe theory [22–24], each molecule experiences a mean field due to long-range attractive pairwise interactions. Properties of the nematic phase can surprisingly be reproduced from an effective orientational potential that ignores short-range repulsive forces (for a discussion see [25]):

$$V(\cos\theta) = -K\langle P_2(\cos\theta)\rangle P_2(\cos\theta) \tag{2}$$

where K is the average strength of molecular interaction, $\langle P_2(\cos\theta)\rangle$ is the order parameter, and $P_2(\cos\theta)$ encompasses the angular dependance of the potential. In the canonical ensemble, the order parameter is thus given by an integral equation involving the orientational distribution function $f(\cos\theta)$ [26]:

$$\langle P_2(\cos\theta)\rangle = \int_0^1 P_2(\cos\theta) f(\cos\theta) d(\cos\theta) \tag{3}$$

$$f(\cos\theta) = \frac{\exp(-\beta V(\cos\theta))}{Z} = \frac{\exp(-\beta V(\cos\theta))}{\int_0^1 \exp(-\beta V(\cos\theta)) d(\cos\theta)} \tag{4}$$

with $\beta = 1/k_B T$. Numerical resolution gives a phase diagram for $\langle P_2(\cos\theta)\rangle$ with respect to T in good agreement with experimental data [26]: in particular, the transition temperature is found to be $T_c = 0.00019 k_B T/K$, and the order parameter displays a small discontinuity at the transition.

In mathematical models, one often considers the stronger approximation in which the molecules have a center of symmetry. Therefore, even though a molecule at space location $\mathbf{r}$ is idealized as a unit vector $\vec{u}(\mathbf{r})$, an order parameter cannot be described by an ordinary vector like in ferromagnets, and following De Gennes [27, 28], one should instead consider a second-rank tensor order parameter (for a detailed discussion on order tensor theories for nematics, see Chapter 4 of [29])

$$Q_{\alpha\beta}(\mathbf{r}) = \frac{1}{N}\sum_{\mathbf{r}'\in\Omega}\left(u_\alpha(\mathbf{r}'-\mathbf{r})u_\beta(\mathbf{r}'-\mathbf{r}) - \tfrac{1}{3}\delta_{\alpha\beta}\right) \tag{5}$$

The sum over the $\mathbf{r}'$'s extends inside a ball Ω around $\mathbf{r}$, of size small, but large compared to microscopic scales.

The $\vec{u}(\mathbf{r})$'s live in a three-dimensional space attached to each real space site, and the $u_\alpha(\mathbf{r})$'s are their Cartesian components. The $\mathbf{r}$'s which locate molecules are ordinary space vectors. Two types of vectors are used, since both $\mathbf{r}$'s and $\vec{u}$'s need not have the same dimensionality (e.g., a film of liquid crystal is naturally described by two-component vectors $\mathbf{r}$'s, which specify the location of three-component $\vec{u}$'s). The tensor $Q_{\alpha\beta}(\mathbf{r})$ has useful properties. It is symmetric and traceless, which reduces the number of its independent components from nine to five. It vanishes in the isotropic phase, and in the nematic phase, it is generally written

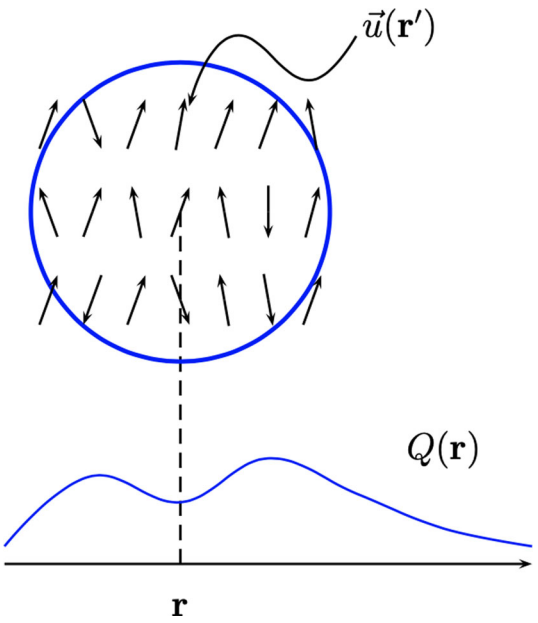

Fig. 2 The definition of the order parameter at the mesoscopic scale

as

$$Q_{\alpha\beta} = Q(T)\left(n_\alpha n_\beta - \frac{1}{3}\delta_{\alpha\beta}\right) \tag{6}$$

where $Q(T)$ is a quadrupolar scalar order parameter that identifies with S for rigid rod-like molecules but that can encompass more general nematogens. For prolate and oblate molecules, it respectively takes the forms

$$[Q_{\alpha\beta}] = \begin{pmatrix} -1/3 & 0 & 0 \\ 0 & -1/3 & 0 \\ 0 & 0 & 2/3 \end{pmatrix} \quad \text{and} \quad [Q_{\alpha\beta}] = \begin{pmatrix} 1/6 & 0 & 0 \\ 0 & 1/6 & 0 \\ 0 & 0 & -1/3 \end{pmatrix} \tag{7}$$

in the principal axes basis.

Being a local order parameter, the object $Q_{\alpha\beta}(\mathbf{r})$ allows for a mean-field description in terms of an expansion of the free energy density known as Landau–de Gennes theory. The approach is based on the assumption that in the vicinity of the phase transition where the order parameter vanishes, it is a small parameter, and the free energy density can thus be expanded in powers of the order parameter. Since there are three independent invariants made from the tensor $Q_{\alpha\beta}$ (these are $\mathrm{Tr}\,(Q)$, $\mathrm{Tr}\,(Q^2)$, and $\det(Q)$), the expansion is built from three leading terms [11, 17, 30]

$$\begin{aligned} F =& F_0 + \int d^3r \Big(\tfrac{1}{2} A(T) Q_{\alpha\beta}(\mathbf{r}) Q_{\beta\alpha}(\mathbf{r}) \\ &+ \tfrac{1}{3} B(T) Q_{\alpha\beta}(\mathbf{r}) Q_{\beta\gamma}(\mathbf{r}) Q_{\gamma\alpha}(\mathbf{r}) \\ &+ \tfrac{1}{4} C(T) (Q_{\alpha\beta}(\mathbf{r}) Q_{\beta\alpha}(\mathbf{r}))^2 \Big). \end{aligned} \tag{8}$$

The first coefficient changes its sign at a temperature called T^*, $A(T) = A_0(T - T^*)$, and B and C are essentially independent of the temperature, and their values can be approximated by those taken at T^*. The small elastic constant limit of Landau–de Gennes theory converges to Frank–Oseen theory [31]. Additional terms are not required if the coefficient of the higher-order term, $C > 0$, which ensures stability of the ordered phase. Further analysis shows that a first-order transition takes place at a temperature T_c slightly above T^*. This phenomenological theory is thus consistent with experimental evidence of a weak first-order transition (in three-dimensional systems).

In real systems, the order parameter is slowly varying in space, and additional terms in the expansion are required, which involve gradients of the order parameter. This is then usually referred to as Ginzburg–Landau theory. This is particularly important in the presence of topological defects which impose specific spatial variations of the molecular orientations in the ordered phase.

The description of the nematic phase has also been extended to non-mean-field approaches. In this perspective, let us mention lattice model studies. As discussed above for the order parameter, in the nematic phase, one can measure the deviation of molecules' individual orientations with respect to the director by the scalar product $\vec{u}_i \cdot \vec{n} = \cos\theta_i$—where the i's are now lattice sites (they play the role of the $\mathbf{r}$'s previously)—but due to the additional local Z_2 symmetry which identifies "heads" and "tails," one cannot distinguish between opposite directions. As a consequence, $\cos(\theta_i)$ vanishes on average while $\cos(\theta_i)^2$ does not and is thus more appropriate for a possible local interaction term. In the disordered phase, the angles are furthermore measured with respect to any arbitrary direction, and the thermal average leads to $\cos\theta_i = 0$ and $\cos(\theta_i)^2 = 1/3$. The quantity $\cos(\theta_i)^2 - 1/3$ thus represents a convenient scalar nearest-neighbor interaction energy. In the literature on liquid crystals, one usually defines this by the second Legendre polynomial, $\phi_i = P_2(\cos\theta_i)$, like for the order parameter. This definition suggests considering lattice Hamiltonians to describe the nematic transition, such as the so-called Lebwohl–Lasher model [32, 33]:

$$-\frac{H}{k_B T} = \frac{J}{k_B T} \sum_{(i,j)} P_2(\vec{u}_i \cdot \vec{u}_j) \tag{9}$$

where the sum is usually restricted to nearest-neighbors in the spirit of studies of critical phenomena. The constant J is an empirical interaction parameter. This model, which is also called the RP^2 model, can be seen as a discrete version of the Maier–Saupe model. It has been (and is still) extensively investigated from Monte Carlo simulations [34–38]. Except for the $\cos(\theta_i)^2$, it looks very similar to the Heisenberg model. Nevertheless, the latter model exhibits a second-order transition in three dimensions, while the Lebwohl–Lasher model displays a first-order transition [32, 39].

Let us stress that the situation sketched above does not apply directly in two-dimensional liquid crystals. The question of the nature of the transition of the Lebwohl–Lasher model is still debated nowadays [40–42], but the role of topological defects there is not under discussion. The situation is either similar to the Kosterlitz–Thouless phase transition [14, 43] which is governed by unbinding of topological defects pairs, or to that of the Heisenberg model for which there is no transition at all, due to the instability of these defects. In all cases, two- or three-dimensional systems, the presence of topological defects is of paramount importance.

2.3 The isotropic–nematic phase transition for pedestrians

The isotropic–nematic phase transition has been a long-standing stumbling block in statistical physics, and since the 1970s, abundant literature has been produced to understand its key mechanisms and its generic properties [17, 30, 44–50]. To grasp the essential features of the isotropic–nematic phase transition, we stick to the Maier–Saupe model and compare the thermal agitation of the aliphatic chains (increasing the mean steric hindrance, e.g., fluidity) to the interaction potential (2) that aligns rigid cores on average along the director field (anisotropy). Maier–Saupe's model leads to similar results as Landau–de Gennes theory, but from rather simpler premises. The nematics in consideration hereafter are thermotropic; for example, the external parameter driving the transition is temperature.[2]

At low temperatures, thermal agitation is weak. Due to the low steric hindrance, nematogens are closer, and van der Waals interactions prevail: the phase is that of a molecular solid (with sometimes a smectic phase in between). The corresponding symmetry groups are discrete. At high temperatures, thermal agitation prevails over molecular interactions: the nematogens are distant from each other, and they form an isotropic fluid. The rotational symmetry group of the phase is $SO(3)$, the group of rotation in three dimensions. Within the intermediate range of temperatures, with a symmetry axis given by $\vec{n}$, its symmetry group is therefore $SO(2) \times Z_2 = O(2)$ (Fig. 3). Therefore, the transition from isotropic to nematic phase involves a spontaneous symmetry breaking.

A thorough inspection of this transition reveals that it is a three-step nucleation mechanism involving [51–53]: (1) the formation of small spherulites where an orientational order arises without correlation with each other, (2) the growth of the ordered domains, and (3) the formation of threads when spherulites have mingled. We also saw that Maier–Saupe theory and the Lebwohl–Lasher model predict a weak discontinuity of the order parameter at T_c. Measurements on different nematic samples also showed the existence of low latent heat, which suggests a first-order transition, but as pre-transitional effects (decay of the dielectric constant with T close to T_c) have also been reported [54], the isotropic–nematic phase transition is in fact weakly first order. Yet having cleared up the nature of the transition does not explain the presence of the threads. This is the object of the next section.

[2] Other possibilities include lyotropic nematics: the external parameter is the concentration of nematogens in a solvent, and the most adequate description is Onsager's model.

2.4 Topology of the isotropic–nematic transition

Topology is the branch of mathematics focusing on the properties that remain unchanged when a topological space is "continuously deformed" (neither torn apart nor punctured). When a topological property changes, it occurs by integer steps, not gradually. Algebraic topology (Poincaré' s former *analysis situs*) seeks algebraic invariants (numbers, abelian groups, rings, etc.) to study and classify topological spaces into equivalence classes. These objects may characterize properties such as the connectedness, the number of holes, and the existence of boundaries. Two manifolds are topologically equivalent or homeomorphic if there exists a bijective and continuous map between them. These two manifolds have to be of the same dimension, as required by Brouwer's invariance of domain theorem. Intuitively, it corresponds to a continuous deformation with no gluing or tearing. Putting it colloquially, for an algebraic topologist, a doughnut is the same thing as a teacup (an object with one hole), but a doughnut is different from a French pretzel (three holes).

Homotopy provides a weaker notion of equivalence between topological spaces than homeomorphism, and it has been used to investigate the properties of singularities in ordered systems such as liquid crystals [55–63], superfluids [55, 64], and the universe [65, 66]. Homotopy corresponds to a continuous deformation where bijectivity is not preserved, i.e., gluing, shrinking, or flattening the space is allowed. For instance, in $\mathbb{R}^2$, a loop (dimension 1) is homotopic to a point (dimension 0). The first homotopy group (or Poincaré group, or fundamental group) is denoted as $\pi_1(\mathcal{M})$, and it tests whether all closed curves (loops) on a manifold $\mathcal{M}$ are homotopic to a point. If this is the case, the fundamental group is trivial, $\pi_1(\mathcal{M}) = 0$. When does this fail? When there are holes! In the aforementioned example, $\pi_1(\mathbb{R}^2) = 0$ but $\pi_1(\mathbb{R}^2 - \{0\}) \neq 0$: removing the origin creates a zero-dimensional (0D) hole in the 2D manifold. Technically, we just used the first homotopy group to test the simple connectedness of $\mathbb{R}^2 - \{0\}$. When $\pi_1(\mathcal{M}) \neq 0$, there are equivalence classes of homotopic loops sharing the same winding number (Whitney–Graustein theorem). The winding number of a regular curve is the number of times the tangent vector fully rotates counterclockwise when going once around the curve. Two closed loops can be attached together to form a new closed loop, which defines the binary operation underlying the group structure [58]. For $\mathcal{M} = \mathbb{R}^2 - \{0\}$, $\pi_1(\mathcal{M}) = \mathbb{Z}$: the equivalence classes consist of loops turning n times around

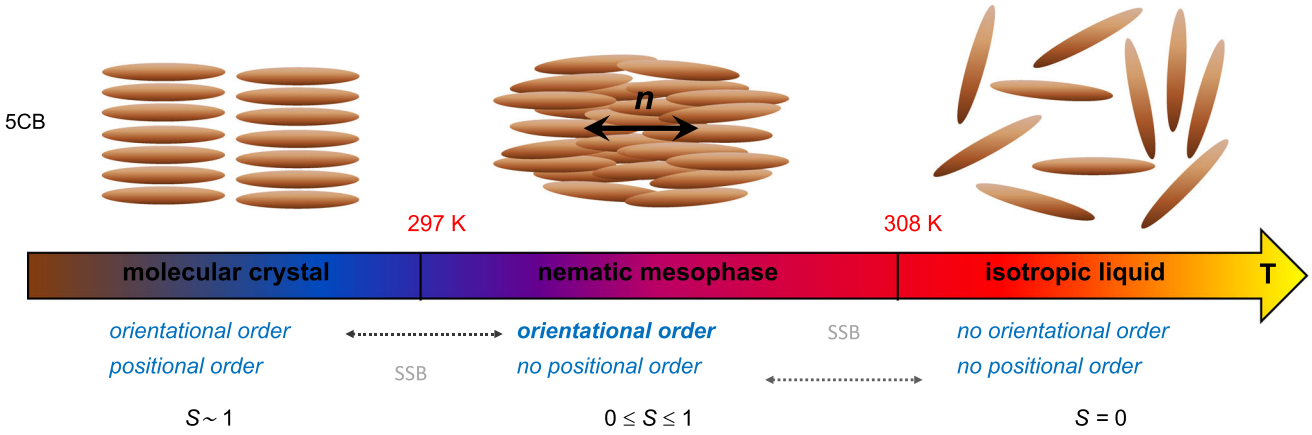

Fig. 3 Phase transitions with 5CB

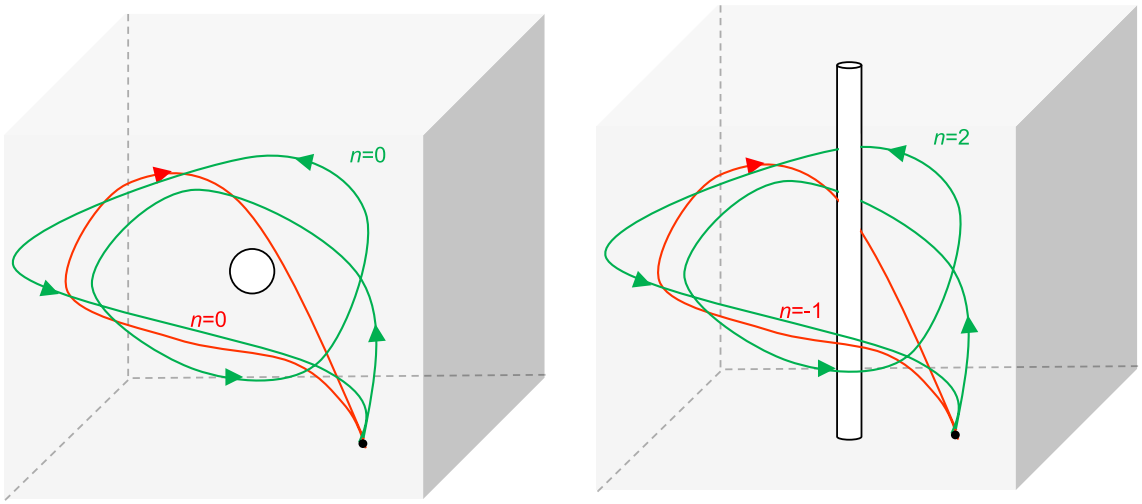

Fig. 4 Left: Trivial closed loops around a 0D hole (white region, spatial extent is for convenience). Right: Some equivalence classes around a 1D hole (white region, spatial extent is for convenience)

the origin (clockwise for $n < 0$, counterclockwise for $n > 0$).

They are many other topological properties than can be tested from homotopy groups: for instance, π_0 tests whether the topological space is path-wise-connected, i.e., if for any pair of points, one can find a path between them that remains in the topological space. Intuitively, it corresponds to the notion of a space that is in one whole piece. In that respect, $\pi_0(\mathbb{R}^2 - \{0\}) = 0$ but $\pi_0(\mathbb{R}^2 - \{x + y = 0\}) \neq 0$: thus, π_0 tests the existence of 1D hole in the 2D manifold. It has to be emphasized that the content of the homotopy group is strongly dependent on the dimension of the manifold: indeed, a 0D hole (or point defect) in a 3D manifold can never be lassoed (see 4), and its fundamental group homotopy is trivial. For $\pi_1(\mathcal{M})$ to be nontrivial, the hole has to be 1D, e.g., a line defect (see Fig. 4). As a rule, we will bear in mind that in dimension p, if the k^{th} homotopy group $\pi_k(\mathcal{M})$ is nontrivial, then topological defects of dimension $p - 1 - k$ appear.

Now, what is the connection of homotopy with phase transitions? This idea is simple: homotopy can predict the kind of order parameter singularities (or topological defects) that can appear after the phase transition from its symmetry-breaking pattern. During a phase transition with a symmetry breaking pattern $G \longrightarrow H$, defects arise according to the topology of the order parameter space defined as the coset $\mathcal{M} = G/H$. The coset notation means that two elements of G can be identified if they differ by an element of H. Intuitively, the coset space G/H corresponds to the information left after noising the elements of G by those of H. For the isotropic–nematic phase, $\mathcal{M} = SO(3)/O(2) = S^2/Z_2$: the order parameter space consists in a 2D sphere having its antipodal points identified. How to make sense of this result from the intuitive view of the coset space? To define an element of $SO(3)$, one needs a rotation angle and a unit vector giving the rotation axis in the 3D space. Now, $O(2) = SO(2) \times Z_2$, and to define an element of $SO(2)$, one needs only an angle, as the axis is set for a rotation occurring in two dimensions. Then, noising the elements of $SO(3)$ by those of $SO(2)$ only leaves information related to the rotation axis. As the surface swept by all possible vectors defining

the rotation axis is the unit sphere, this means that $SO(3)/SO(2) = S^2$ and therefore that $\mathcal{M} = S^2/Z_2$. Such an object is known as the real projective plane and can be visualized from its immersion in 3D space, the Boy surface [67, 68]. The contents of the different homotopy groups are ([59]) as follows:

- $\pi_0(\mathcal{M}) = 0$: one cannot observe surface defects in nematics.
- $\pi_1(\mathcal{M}) = Z_2$: one can observe line defects in nematics, and they are precisely the thread-like structures we were trying to explain since the previous section. Z_2 is the additive group of integers modulo 2, and in such a group, $1 + 1 = 0$. This means that a line defect is its own "antidefect": when two identical line defects meet, they are annihilated, as we will see in more details below. These objects are generically called disclinations, and Friedel gave its name to the nematic phase after them (in Greek, $\nu\eta\mu\alpha$ means thread).
- $\pi_2(\mathcal{M}) = \mathbb{Z}$: point-like defects (called hedgehogs) appear in nematics [69]. The additive group of integers, $\mathbb{Z}$, means that there is an infinite class of point defects. Each defect is characterized by an integer, called the topological charge, which represents the strength of the defect. Similarly to the electric charge in electrostatics, there are positive and negative point defects that are annihilated when they meet.
- $\pi_3(\mathcal{M}) = \mathbb{Z}$: textures such as skyrmions and hopfions appear in nematics [70, 71]. There is also an infinite class of textures, the topological charge of which counts the integer number of times the field configuration wraps around itself [72, 73].

In the remainder of this work, we will narrow our focus to line defects, mostly because of the specific role they play in different branches of physics.

3 Topological defects, a common pattern of nematics

3.1 Typology of disclinations

Let us look closer at the homotopy content of the first fundamental group. The two equivalence classes for the addition law are $\pi_1(\mathcal{M}) = Z_2 = \{0, 1\}$. The equivalence class associated to the neutral element 0 corresponds to ordinary closed paths on the manifold (see the green loop in Fig. 5): as they can be shrunk to a point, they correspond to removable singularities called wedge disclinations. But the particular structure of the Boy surface allows for another kind of loop: an open curve connecting two antipodal points (see the red curve in Fig. 5). Obviously, there is no way to shrink the curve into a point while maintaining its closure: such a singularity is topologically stable and is called a Mœbius disclination. These two categories of defects combine according to the algebra of Z_2: $0+0 = 0$, $0+1 = 1$, and $1 + 1 = 0$. For instance, in the latter case, this means that two open curves connected at the same antipodal points form a larger loop that can be shrunk to a point.

To go further in the description of these singularities, let us build the Frank–Oseen elastic free energy. Consider a given director field $\vec{n}_0(\mathbf{r})$. Deformations about that configuration are orthogonal to it as $\vec{n}_0.\vec{n}_0 = 1$, which leads to $\vec{n}_0.\delta\vec{n} = 0$. To set things up, one considers $\vec{n}_0 = \vec{e}_3$, which then demands $\delta\vec{n} = (\delta n_1, \delta n_2, 0)$. A Taylor expansion of $\delta\vec{n}$ reveals three deformation modes:

- a splay mode in $\vec{\nabla}.\vec{n}$
- a twist mode in $\vec{n}.(\vec{\nabla} \times \vec{n})$
- a bend mode in $\vec{n} \times (\vec{\nabla} \times \vec{n})$

Similar to the harmonic oscillator, the (simplest) Frank–Oseen free energy density describing nematoelasticity is quadratic with respect to the deformation, and it is written as

$$f[\vec{n}] = \frac{K_1}{2}|\vec{\nabla}.\vec{n}|^2 + \frac{K_2}{2}|\vec{n}.(\vec{\nabla} \times \vec{n})|^2 + \frac{K_3}{2}|\vec{n} \times (\vec{\nabla} \times \vec{n})|^2 \tag{10}$$

with K_i the corresponding elastic constants.

In the one-constant approximation, $K_1 \approx K_2 \approx K_3 = K = E_0/L$. Typically, one has $E_0 \approx 0.1$ eV, $L \approx 1$ nm, which gives $K \approx 10^{-11}$ N (verified for 5CB). Moreover, for planar configurations of the director field, $\vec{n} = \cos\psi\,\vec{e}_1 + \sin\psi\,\vec{e}_2$. The Frank–Oseen free energy density thus simplifies as

$$f[\vec{n}] = \frac{K}{2}|\vec{\nabla}\psi|^2 \tag{11}$$

Minimizing f and retaining the director field configurations which do not depend on the radius finally gives $d^2\psi/d\theta^2 = 0$, that is,

$$\psi(\theta) = m\theta + \psi_0 \tag{12}$$

where m and ψ_0 are real constants. As the direction of $\vec{n}$ must be well defined at each point, one has the constraint

$$\oint_\theta d\psi = 2\pi m = k\pi \quad k \in \mathbb{Z}. \tag{13}$$

The constraint $k \in \mathbb{Z}$ is a result of Z_2 symmetry. This means that (1) m is a winding number and (2) its values are restricted to $m = \pm 1/2, \pm 1, \pm 3/2, \pm 2....$ Substituting into (11), the free energy is now in m^2, which means that in practice, only distortions with the lowest winding numbers are observed.

In Fig. 6, several disclinations are plotted for different values of m and ψ_0. The vortex and the aster configurations are topologically equivalent, as they can be transformed into each other by a continuous rotation of the director field from 0 to $\pi/2$: this means they belong

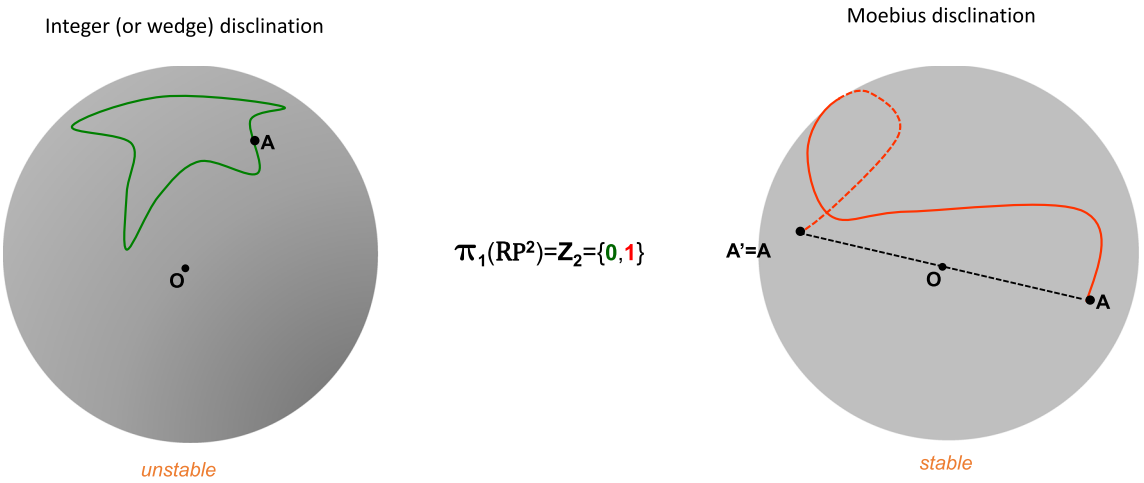

Fig. 5 The two equivalence classes of π_1 on the Boy surface

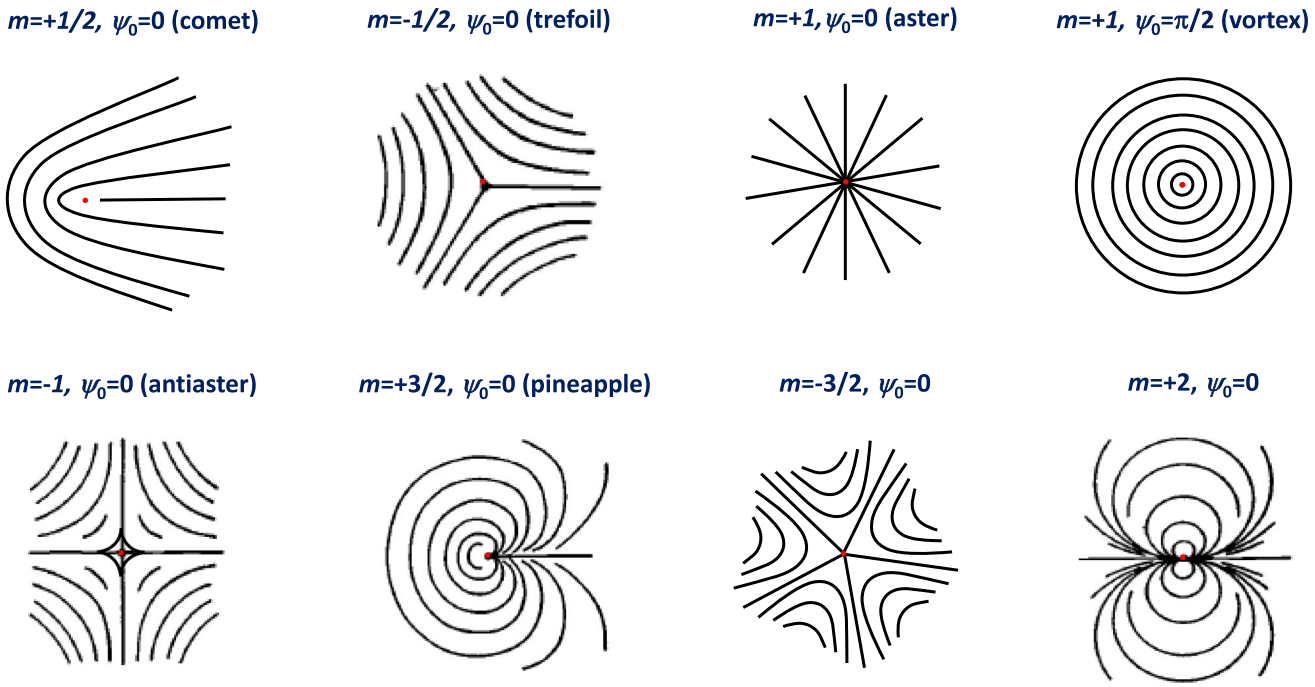

Fig. 6 Examples of director field distributions for several planar line defects. The black continuous curves are the director field lines tangent at each point to $\vec{n} = (\cos\psi, \sin\psi)$, and the core singularity is in red. The antiaster and antivortex configurations are identical up to a $+\frac{\pi}{4}$ rotation. Adapted from [11]

to the same equivalence class. In fact, the director field of these defects can even deform continuously to relax into a non-singular configuration (escape into the third dimension): these defects are topologically unstable (this would not be true for two-component order parameter $\vec{n}$ [74]). As the same goes for $m = -1$ defects, one infers that disclinations of integer strengths belong to the trivial equivalence class (denoted as $N = 0$) of π_1. On the contrary, disclinations of half-integer strengths are not topologically removable, and they belong to the other equivalence class (denoted as $N = 1$). Although m is sometimes called the topological charge of the defect, it is the absolute value of m that really matters for topology.[3]

[3]The sign of m can be distinguished by the rotation of the crossed polarizers. Indeed, polarizing microscopy reveals Schlieren patterns, for which the number of dark brushes is $4|m|0$. Dark brushes from a positive (negative) defect rotate in the direction the same as (opposite to) that of the polarizers.

3.2 Geometry of line defects

From the standpoint of optics, nematics behave as uniaxial media. Their permittivity is $\varepsilon_\parallel$ in the direction of $\vec{n}$ and $\varepsilon_\perp$ in perpendicular planes. Seeking solutions in terms of plane waves shows that such media support two optical modes: the ordinary wave, corresponding to a regular dispersion relation with refractive index $n_0 = \sqrt{\varepsilon_\perp}$, and the extraordinary wave, for which the ray index is anisotropic:

$$N_e(\mathbf{r}) = \sqrt{\varepsilon_\perp \cos^2\beta(\mathbf{r}) + \varepsilon_\parallel \sin^2\beta(\mathbf{r})} \tag{14}$$

with $\beta(\mathbf{r})$ the angle between the director and the tangent vector to the ray. Propagation of the extraordinary light is ruled by the Fermat–Grandjean principle established in 1919 [11]: as $\vec{n}$ varies from point to point, so does N_e, and light is expected to follow curved paths.

There is another well-known area in physics where light paths are curved: general relativity (for a modern textbook, see the excellent [75]). Gravity is nothing more that the effect of spacetime curvature on the dynamics of massive and massless objects. For instance, in the vicinity of a massive star, light undergoes a gravitational lensing which bends its trajectory (this property was the first prediction of general relativity that was tested by Eddington in the same year, 1919). The mathematical tool used to study curved spacetimes is differential geometry, most notably developed by Riemann. In the presence of curvature, all known laws of Euclidean geometry are shaken up. For instance, Pythagoras' theorem, usually written as $ds^2 = dx^2+dy^2+dz^2$ for infinitesimal triangles, is now written as[4]

$$\begin{aligned} ds^2 = {} & g_{11}dx^2 + g_{22}dy^2 + g_{33}dz^2 + 2g_{12}dxdy \\ & + 2g_{13}dxdz + 2g_{23}dydz = \sum_{i,j=1,3} g_{ij}dx^i dx^j \end{aligned} \tag{15}$$

The weighting coefficients g_{ij} are the components of a second-order tensor, called the metric, which can be seen as the multiplication table of the basis vectors chosen to describe the problem. In gravity, the metric is four-dimensional and is a solution of Einstein's field equations that relate the geometry to the mass-energy content.

How to extract a metric description for liquid crystals? This question was successfully addressed in [76–78], and we will sum up here the recipe to be followed:

1. Consider a light path parameterized by ℓ and express the tangent vector in the Cartesian basis

$$\vec{r} = r\cos\theta\,\vec{e}_x + r\sin\theta\,\vec{e}_y \tag{16}$$

$$\vec{T} = \frac{d\vec{r}}{d\ell} = \left(\dot{r}\cos\theta - r\dot{\theta}\sin\theta\right)\vec{e}_x + \left(\dot{r}\sin\theta + r\dot{\theta}\cos\theta\right)\vec{e}_y \tag{17}$$

   Here the dot is a shorthand notation for $d/d\ell$.
2. Compute the components of $\vec{n} = \cos\psi\,\vec{e}_x + \sin\psi\,\vec{e}_y$ with respect to $\vec{T}$:

$$\vec{T}.\vec{n} = \dot{r}\cos(\psi-\theta) + r\dot{\theta}\sin(\psi-\theta) \tag{18}$$

$$|\vec{T}\times\vec{n}| = -\dot{r}\sin(\psi+\theta) + r\dot{\theta}\cos(\psi-\theta) \tag{19}$$

3. Replace in the Fermat–Grandjean line element and see the defect metric appear (to spare lengthy calculations, one will consider the aster defect for which $\cos\beta = \dot{r}$ and $\sin\beta = r\dot{\theta}$):

$$\begin{aligned} ds^2 &= N_e^2(\vec{r})d\ell^2 \\ &= \left(\varepsilon_\perp\dot{r}^2 + \varepsilon_\parallel r^2\dot{\theta}^2\right)d\ell^2 \\ &= \varepsilon_\perp dr^2 + \varepsilon_\parallel r^2 d\theta^2 \end{aligned} \tag{20}$$

Adding the z term and performing a simple rescaling of the radial coordinate finally leads to the 3D line element

$$ds^2 = dr^2 + \alpha^2 r^2 d\theta^2 + dz^2 \tag{21}$$

where $\alpha = \sqrt{\frac{\varepsilon_\parallel}{\varepsilon_\perp}}$.

What kind of geometry does this represent? A first hint is obtained by computing the Ricci scalar

$$R(r) = \frac{1-\alpha}{\alpha r}\delta(r) \tag{22}$$

The geometry is therefore flat everywhere but on the z-axis. Moreover, considering a circle of unit radius about the z-axis, the perimeter is given by $p = \oint ds = 2\pi\alpha$. These two elements indicate that when $\alpha < 1$, the geometry is conical, as described by a Volterra cut-and-glue process (see Fig. 7).

For the sake of completeness, we also report the line element corresponding to a general (m, ψ_0)-disclination line [76]:

$$\begin{aligned} ds^2 = {} & \left(\cos^2[(m-1)\theta+\psi_0] + \alpha^2\sin^2[(m-1)\theta+\psi_0]\right) \\ & + \left(\sin^2[(m-1)\theta+\psi_0] + \alpha^2\cos^2[(m-1)\theta+\psi_0]\right) \\ & - \left(\alpha^2-1\right)\sin[2(m-1)\theta+2\psi_0] + dz^2 \end{aligned} \tag{23}$$

[4] For the sake of simplicity, we omitted the time component, but in relativity, one must bear in mind that time and space are put on an equal footing, and the real interval must involve quadratic terms in cdt, with c the speed of light.

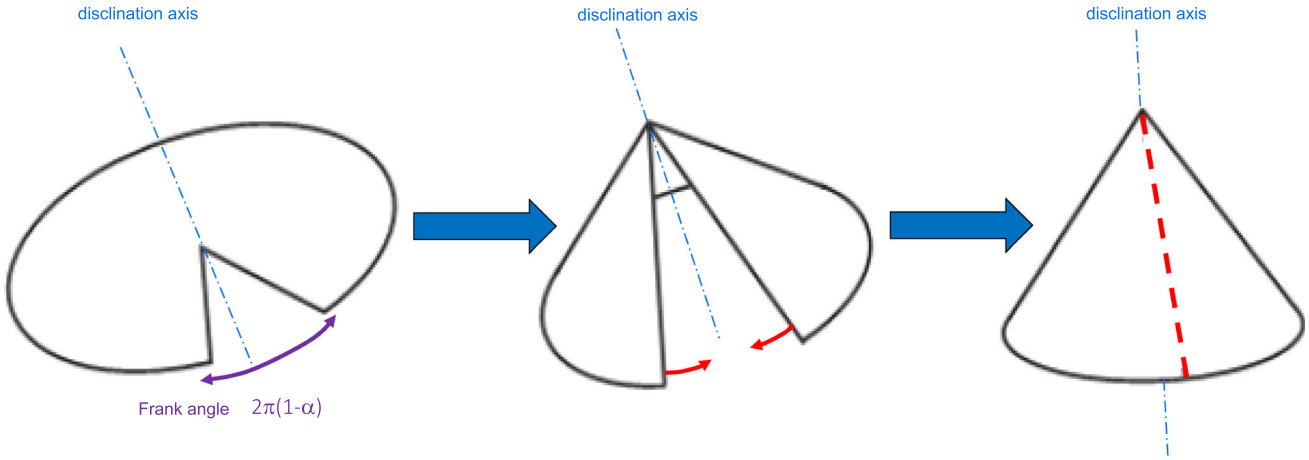

Fig. 7 Two-dimensional view of the Volterra process for generating a wedge disclination with $\alpha < 1$

3.3 Anholonomy

Topological defects generate curved geometries, and therefore, one may expect many physical outcomes of incoming fields, the most natural being lensing effects [76, 77] and scattering [78, 79]. This can be easily understood from the geodesic equations, which provide the shortest and autoparallel paths in a purely curved geometry (no torsion[5]). Writing the parallel transport of the tangent vector along a curve gives

$$\frac{d^2x^i}{dt^2} + \Gamma^i_{jk}\frac{dx^j}{dt}\frac{dx^k}{dt} = 0 \tag{24}$$

where Γ^i_{jk} are the Christoffel symbols of the second kind:

$$\Gamma^i_{jk} = \frac{1}{2}g^{il}(\partial_j g_{kl} + \partial_k g_{jl} - \partial_l g_{jk}) \tag{25}$$

Geodesics correspond to the actual light paths, and for the background metric (21), integration leads to

$$r(\theta) = \frac{C}{\alpha\sqrt{E}}\sqrt{1 + \frac{\tan^2(\alpha\theta - F)}{2}} \tag{26}$$

where C, E, and F are integration constants (for graphical representations, see for instance [76, 80]).

More subtle but yet related to parallel transport is the emergence of anholonomy effects, on which we will now focus our attention. Let us consider first a practical problem (see Fig. 8): a world traveler living in France (point A) wants to explore the north pole. He can either go directly to the north by following the prime meridian up to point C, or he can detour via Québec (point B) and head north to C along the 70° W parallel. If he compares his compass needle in the two trips, he will discover a strange result: even if he parallel-transported in each circuit from the same starting and ending points, the direction vector at C is not the same. Stated otherwise: after a closed loop, a parallel-transported vector fails to recover its initial direction by a mismatch angle $\hat{h}$. This phenomenon is called anholonomy.

Intuitively, anholonomy can be understood as a topological effect. Girard's formula establishes the connection between the surface Σ enclosed by circuit ABC and the Gauss curvature of the 2-sphere $F = 1/R^2$:

$$\Sigma = R^2\Omega = \frac{\hat{A} + \hat{B} + \hat{C} - \pi}{F} \tag{27}$$

In the case depicted in Fig. 8, this simplifies into $F\Sigma = \hat{C}$, which also turns out to be the mismatch angle $\hat{h}$: this latter is thus a measure of the Gaussian curvature F of the surface Σ bounded by the closed circuit. Such result is an basic outcome of the Ambrose–Singer theorem: for a given connection on a vector bundle[6], the curvature corresponds to the surface density of holonomy. Now, Gaussian curvature is also related to the topology of the surface via the Gauss–Bonnet theorem:

$$\iint_\Sigma F dS + \oint_{\partial\Sigma} \kappa_g ds = 2\pi\chi \tag{28}$$

Here, χ is the Euler–Poincaré characteristic (topology), and κ_g is the geodesic curvature. For the lost traveler

[5] Like curvature, torsion is a property of the connection (actually this is the antisymmetric part of the connection and it vanishes in the case of a Levi–Civita connection, this is why general relativity does not deal with torsion). When torsion vanishes, geodesic ("shortest") lines are also autoparallel ("straightest," i.e., lines along which the tangent vector is parallel-transported via the connection).

[6] Vectors at a point x of a manifold live in the tangent space at x. The tangent spaces at neighboring points are different vector spaces, and the vector bundle is understood as the collection of them. The connection is the object which allows us to transport or compare vectors at different points [161].

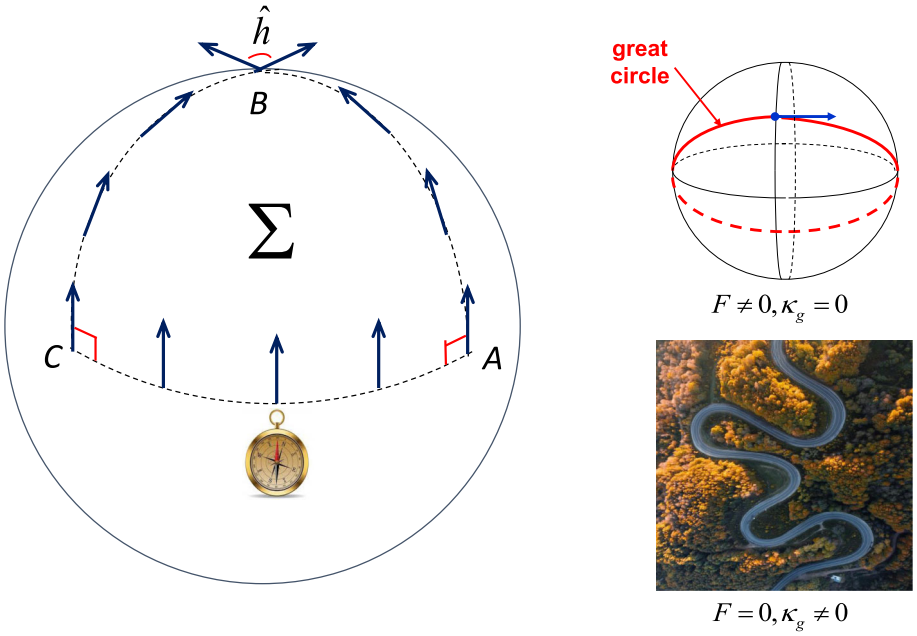

Fig. 8 Left: The world traveler problem. Right: Difference between Gauss curvature (top) and geodesic curvature (bottom) on Earth (2-sphere). Even if a traveler follows the straightest paths (roads of zero geodesic curvature), they will always experience the Earth's Gaussian curvature along them (red paths or geodesics of the 2-sphere)

problem, this simplifies into $\hat{h} = 2\pi\chi$, which establishes the topological origin of anholonomy.

A more formal and general expression of anholonomy has been obtained by Elie Cartan from the definition of parallel transport and is summed up in a modern form in [75]. Let there be a path parameterized by λ along which a vector $\mathbf{V}$ is parallel-transported. The parallel propagator Π is defined as

$$V^{\mu}(\lambda) = \Pi^{\mu}_{\ \rho}(\lambda) V^{\rho}(0) \tag{29}$$

The parallel transport condition applied to $\mathbf{V}$ is written as

$$\frac{d}{d\lambda} V^{\nu}(\lambda) = -\Gamma^{\nu}_{\sigma\mu} \frac{dx^{\sigma}}{d\lambda} V^{\mu}(\lambda) = A^{\nu}_{\ \mu}(\lambda) V^{\mu}(\lambda) \tag{30}$$

where Γ are Christoffel's connection symbols. This leads to the following equation for the propagator

$$\frac{d}{d\lambda} \Pi^{\nu}_{\ \rho}(\lambda) = A^{\nu}_{\ \mu}(\lambda) \Pi^{\mu}_{\ \rho}(\lambda) \tag{31}$$

This formally integrates into

$$\Pi^{\mu}_{\ \rho}(\lambda) = \delta^{\mu}_{\rho} + \int_0^{\lambda} A^{\mu}_{\ \sigma}(\eta) \Pi^{\sigma}_{\ \rho}(\eta) d\eta \tag{32}$$

and can be solved iteratively. Instead of integrating over n-simplices, one integrates over n-cubes while keeping the product in the right order, to get the simpler expression:

$$\Pi^{\mu}_{\ \nu}(\lambda) = \mathrm{P} \exp \int_0^{\lambda} A^{\mu}_{\ \nu}(\eta) d\eta \tag{33}$$

where P is the ordering operator. On a loop γ about a point M, the anholonomy is written explicitly as

$$\Pi^{\mu}_{\ \nu}[\gamma] = \mathrm{P} \exp\left(- \oint_{\gamma(M)} \Gamma^{\mu}_{\sigma\nu} dx^{\sigma} \right) \tag{34}$$

As expected from the Ambrose–Singer theorem, to know the holonomy at every point of the manifold is equivalent to knowing the curvature at every point of the manifold: this property is heavily used in quantum loop gravity.

Now, let us establish the anholonomy due to a disclination [81]. For a loop about the origin in a $z = C^{st}$ plane, only the polar connection symbol is retained:

$$\Gamma_{\theta} = \frac{m}{\alpha} \left(\alpha^2 \cos^2 \left[(m-1)\theta + \psi_0 \right] + \sin^2 \left[(m-1)\theta + \psi_0 \right] \right) \begin{pmatrix} 0 & 1 \\ -1 & 0 \end{pmatrix} \tag{35}$$

For instance, for the aster disclination, this reduces to $\Gamma_{\theta} = \begin{pmatrix} 0 & \alpha \\ -\alpha & 0 \end{pmatrix}$, and the parallel propagator becomes

$$\Pi^{\mu}_{\ \nu}[\gamma] = \begin{pmatrix} \cos(2\pi\alpha) & -\sin(2\pi\alpha) \\ \sin(2\pi\alpha) & \cos(2\pi\alpha) \end{pmatrix} \tag{36}$$

When parallel-transporting a vector around it, the disclination causes an active rotation of angle $-2\pi\alpha$. All in all, the global mismatch angle when a vector describes a loop around the defect is $\hat{h} = 2\pi - 2\pi\alpha$. This means that disclinations generate a classical analog of the Aharonov–Bohm effect. Indeed, the curvature is confined within the disclination line and vanishes everywhere else, but it has measurable effects affecting

the phase of neighboring objects. This is one among many examples of what is generically called geometric or Berry phases, that is, "phases are not attributed to the forces applied onto the [quantum] system. Instead, they are associated with the connection of space itself" [82].

4 Topological defects, a universal pattern of nature?

4.1 Biology

a. A tentative definition To begin with, we will discuss how a statistical physicist may describe biological systems. To do so, we will first need to address one question: what does it mean for a system to be at equilibrium? Figuring out what equilibrium means is not as simple as it appears at first glance. For instance, is the glass of my window at equilibrium or not? In his lectures on statistical physics, RP Feynman defined equilibrium as the situation when "all the fast things have happened but the slow things have not" [83]. As handy as it sounds, this definition is yet incomplete as it blurs the demarcation between an equilibrium state and a nonequilibrium steady state. A better criterion to discriminate equilibrium from out-of-equilibrium situations is for a system to be crossed by fluxes, for example, of matter or energy, exchanged with its surrounding. The glass of a window is nowadays understood as a metastable super-cooled liquid that flows because of gravity, but with relaxation times averaging $\tau \approx 10^9$ years (for water, τ is of the order of milliseconds). The glass of my window is therefore crossed by fluxes of matter, and it is in a nonequilibrium steady state.

Living biological systems are out of equilibrium as well. For instance, a living cell consumes energy to maintain homeostasis (a nonequilibrium steady state) and perform mechanical work such as cellular division, membrane transport (water molecules sneak out the membrane as the phospholipid bilayer flexes and bends), and motility (motion of flagella). From the standpoint of statistical mechanics, to be dead means to be at thermodynamic equilibrium. But contrary to the aforementioned nonliving examples, the nonequilibrium steady state is not driven by external macroscopic fields, but by its internal components: animals in a flock, molecular motors, and microtubules for cells [84–86]. For the statistical physicist, biology is the study of active matter, for example, nonequilibrium self-organized systems which do not couple trivially to the energy input from their environment [87]. Examples of active matter include colonies of bacteria, assemblies of myocyte cells, flocks of sheep, schools of fish. Most of the time, the basic bricks comprising active matter are strongly anisotropic, such that the whole system displays a nematic order. Hence, at places where the average orientation of these bricks is ill-defined, topological defects arise.

b. Active turbulence as a defect factory Let us now investigate additional peculiarities of active matter by examining how it evolves in time. Usually, ordinary isotropic liquids obey the famous Navier–Stokes equations[7]

$$\rho \frac{D\mathbf{V}}{Dt} = \rho \mathbf{g} + \boldsymbol{\nabla}.\bar{\bar{\boldsymbol{\sigma}}} \tag{37}$$

where the left-hand-side inertial terms include D/Dt, the material derivative, and ρ, the mass density. The right-hand side includes $\mathbf{g}$, the gravitational acceleration at Earth's surface, and $\bar{\bar{\boldsymbol{\sigma}}} = -p\bar{\bar{\mathbf{I}}} + 2\eta\bar{\bar{\mathbf{D}}}$, the Cauchy stress tensor, which encompasses contributions due to the pressure p and to the fluid viscosity η ($\bar{\bar{\mathbf{D}}}$ stands for the strain rate tensor). The ratio between inertial terms and viscous forces defines a dimensionless quantity, the Reynolds number (originally introduced by George Stokes [88]): at low Reynolds numbers, flows are laminar (regular and reversible), but at high Reynolds numbers, flows become turbulent (chaos and non-reversibility) [89].

In anisotropic liquids such as nematics, the fluid flow is furthermore coupled to the orientational order, which imparts them with unusual rheological features, such as the dewetting behavior of thin films, the presence of topological defects, or backflow. Under the effect of an entering mass flow, the velocity field inside a nematic generates shear stresses that rotate the rodlike molecules and hence the director field. This mechanism is called advection [11]. Conversely, let us submit a nematic at rest to an external electric field. For steric reasons, a rotation of the director exerts a shear stress on neighboring molecules which puts them into motion: this is called backflow [11]. The complete set of equations governing nematohydrodynamics (including advection and backflow terms) form the Beris–Edwards model[8]:

$$\rho \frac{D\mathbf{V}}{Dt} = \rho \mathbf{g} + \boldsymbol{\nabla}.\bar{\bar{\boldsymbol{\sigma}}} \tag{38}$$

$$\frac{D\bar{\bar{\mathbf{Q}}}}{Dt} = \Gamma\bar{\bar{\mathbf{H}}} + \bar{\bar{\mathbf{S}}} + \lambda\bar{\bar{\mathbf{Q}}} \tag{39}$$

where Γ is the rotational diffusion constant, $\bar{\bar{\mathbf{Q}}}$ is the Landau–de Gennes order parameter tensor, $\bar{\bar{\mathbf{H}}}$ is the molecular field (driving relaxation towards a minimum of free energy), and $\bar{\bar{\mathbf{S}}}$ is the advection term. Compared to Newtonian hydrodynamics, the Cauchy tensor in (39) includes an extra term corresponding to backflow. Passive nematics can relax to configurations where the elastic energy is minimal: the medium then reaches a rest state after the decay of topological defects.

[7] Finding general regular solutions of these equations is still one of the Millennium open problems listed by the Clay Institute.

[8] There is also another set forming the Ericksen–Leslie equations, which are simpler but limited to uniaxial media and to smooth variations of the nematic ordering.

A nematic becomes active as a result of many couplings with its environment (for a review see [91]). For instance, the complex motions of a school of sardines occur because each fish draws energy from marine plankton it ingested (energy couplings), but they can also respond to the presence of natural predators, local modifications of the sea properties, etc. Every time, the energy fed at the individual scale (bacteria, cell, sheep, fish, etc.) is transformed into organized motion at large scales. In many ways, this can be understood as a reverse Richardson cascade: contrary to ordinary turbulence where energy is transferred from large kinetic scales to small dissipative scales [89], the energy transfer occurs bottom-up. Active nematohydrodynamics is thus about the collective dynamics of energy-transducing anisotropic units [84], and the changes in Beris–Edwards equations consist in adding two extra terms: (1) a linear source term $\lambda\bar{\bar{\mathbf{Q}}}$ in (38) and (2) a new activity term $-\zeta\bar{\bar{\mathbf{Q}}}$ in the Cauchy tensor [92]. These new terms result in a cyclic process: hydrodynamic instabilities generate surface singularities that fluctuate and decay into linear topological defects (mostly comets and trefoils, see Fig. 6), then defect–antidefect pairs are annihilated (according to the algebra of Z_2), which in turn generates hydrodynamics instabilities, etc. The proliferation of both line defects and vortices corresponds to a chaotic nonequilibrium steady state for low Reynolds numbers [84, 93–96]. We will next discuss several biological mechanisms in which disclinations play a crucial part.

c. Ethology, morphogenesis, and oncology Comet- and trefoil-like defects behave quite differently from the standpoint of elasticity. Doostmohammadi et al. [91] both computed and measured the stress distribution in the vicinity of these two kinds of defects (see Fig 9). The directions where gradients are maximum correspond to the symmetry axis of the director field distributions. Averaging the stress contributions in the plane shows that there is a large net force associated to the comet which is oriented towards the head of the comet. On the contrary, for the trefoil, the resulting net force is very low (theoretically, it vanishes if the sample is axisymmetric). In recent decades, our understanding of the delicate mechanisms involved in the functioning of organs has made substantial progress. Cells are now understood as highly sensitive mechanotransductive units, displaying an orientational order due to the elongated structures (actin and intermediate filaments, microtubules) forming the cytoskeleton. It must be remarked that actin and microtubules may also form polar organic materials [97], in which the formation of ± 1 wedge disclinations is energetically favored. Hence, a topological defect causing a singularity in the orientational order, i.e., in the stress distribution, is likely to trigger several biological responses, driving processes such as the dynamics of animal groups, morphogenesis, or disease initiation [97].

Colonies of bacteria, insect swarms, and schools of fish all behave as active nematics, as they are essentially assemblies of anisotropic motile units. The effect of Mœbius defects on bacteria populations seems well captured. References [98, 99] found that in a lyotropic liquid crystal (disodium cromoglycate), the populations of *Bacillus subtilis*—a common plant growth-promoting rhizobacteria from the soil—swim from trefoil-like defect cores to comet-like defect cores. Similarly, [100] showed that colonies of *Myxococcus xanthus*, another common rod-like bacteria living in the soil, may form new cell layers at $+1/2$ defects and holes at $-1/2$ defects (competition between different colonies also showed that $+1/2$ defects help a colony in prevailing over another [101]). For larger animals such as insects, fish, and birds, the role attributed to defects is not as clear because of nonlinear processes [102]. A recent work dealing with a colloidal liquid suggests that the remarkable flow stability of flocking matter could come from the self-advection and density gradient around -1 topological defects [103].

Morphogenesis and vesicle growth have recently been understood as processes driven by topological defects [104, 105]. The reason for this is at the interplay between mechanics, soft matter physics, and topology. Many living systems have an outer layer rich in actin filaments and microtubules, which provides them with an orientational order. Due to the Poincaré–Brouwer theorem (sometimes called the "hairy ball theorem"), lines covering any closed curved surface present at least one singular point, where tangent vectors are ill-defined (the global topological charge in a spheroid is set at $+2$): this explains the presence of cyclonic vortices at the Earth's surface or rebellious cowlicks on someone's head. For a biological organism topologically equivalent to a 2-sphere, the hairy ball theorem states that topological defects are unavoidable on its surface. Keber et al. [106] showed that defect sites on a spherical vesicle rich in microtubules were precursors for the growth of protrusions. Cell differentiation and swirling protrusions have recently been reported to be driven by integer defects (spirals and asters) in myoblast monolayers [105, 107], known to be rich in actin and myosin. Reference [108] investigated the biophysics of hydra, a small freshwater predatory animal that is almost immortal as it can regenerate each organ (head, foot, mouth, tentacles). After being cut into pieces, each part folds into a spheroid that supports topological defects. Due to the nematic actin organization, differentiation and regeneration occur at protrusions growing from defect sites, the topological charge being associated to one and only kind of organ ($+1$ for mouth, foot, and tentacle, $-1/2$ for the base).

Mœbius defects may also play a important part in oncology. The transcription coactivator called YAP (yes-associated protein) is known to promote tumorigenesis, metastasis, and even chemotherapy resistance [109–114]. YAP is also critical in cell death mechanisms (such as apoptosis and ferroptosis) and cell extrusion from biological tissues (see [115] for a recent review). Hence, in principle, it should be possible to use YAP to trigger cancer cell death. And this is precisely where topological defects come into play: high levels of compressive stresses at the head of comet-like defects are

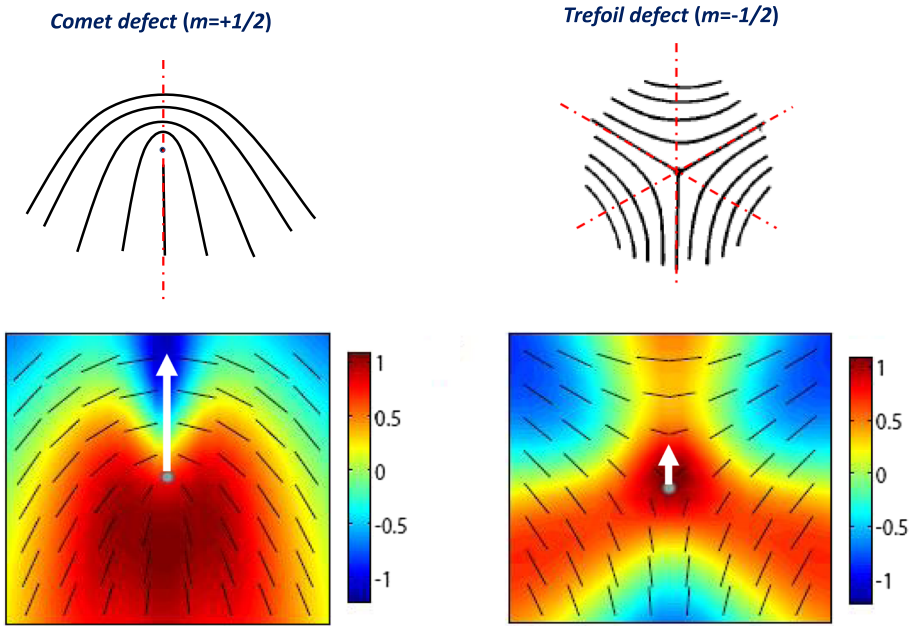

Fig. 9 Upper left: Director field for a comet-like disclination (one symmetry axis in the red dotted line). Lower left: Stress field around the comet (normalized units). Large net resulting force in white as a result of stress gradients (adapted from [91]). Upper right: Director field for a trefoil-like disclination (three symmetry axis in the red dotted line). Lower right: Stress field around the trefoil (normalized units). Small net resulting force in white as a result of stress gradients (adapted from [91])

known to translocate YAP from the nucleus to the cytoplasm and to trigger cellular death and extrusion [97, 116]. However, the journey to defect-engineered therapies based on YAP deactivation promises to be long, as competing mechanisms involving defect-induced cell motions have recently been reported to impede malignant cell clearance [117].

4.2 Cosmology and cosmic strings

a. Phase transitions in cosmology According to the Standard Hot Big Bang Model, about 13.8 billion years ago, our universe was in an extremely hot dense state, consisting in a quark-gluon plasma. In the framework of grand unified theory, the four fundamental interactions were supposed to be unified, the corresponding "superforce" being invariant under the element of a grand unified gauge symmetry group G. Then, the universe expansion played the role of a gigantic Joule–Thomson expansion, which caused large temperature drops likely to give rise to cosmological phase transitions with spontaneous gauge symmetry breaking (SSB). After the last of these transitions occurred (electroweak phase transition) at about 10^2 GeV, the electroweak force split up into the electromagnetic force and the weak nuclear force, which corresponds to the gauge symmetry $SU(3)_c \times U(1)_{em}$. As in condensed matter, the topology associated to the symmetry-breaking pattern provides information on the possible topological defects that may appear. Only the terminology is changing: instead of the order parameter space, one speaks of the vacuum manifold, which is the set of Higgs field configurations minimizing energy modulo gauge transformations. Jeannerot et al. [118] determined the homotopy content corresponding to all eligible groups G likely to decay below 10^{16}GeV into $SU(3)_c \times SU(2)_L \times U(1)_Y$. Their conclusion leaves no doubt concerning the formation of cosmic strings: "among the SSB schemes which are compatible with high energy physics and cosmology, we did not find any without strings after inflation" [118].

Of prime importance is the phase of cosmic inflation that presumably happened at the very beginning of the universe [120]. It consists in an extremely rapid expansion (typically a factor 10^{26} within 10^{-32} seconds) likely to solve cosmological riddles such the horizon and flatness problems [121]. From the point of view of statistical physics, inflation is nothing more than a tremendous quench, and it is likely to promote the formation of topological defects. Kibble [122] and later Zurek [123] proposed a mechanism now known as the Kibble–Zurek scenario (KZS) describing the different steps of this quench. It starts with a nucleation process, similarly to what happens at the isotropic–nematic phase transition, but the orientational order comes from the phase choice of a complex scalar field generically called a Higgs field. The fast temperature drop due to inflation causes the Higgs field to locally take a non-vanishing vacuum expectation value and hence to make a phase choice (see Fig. 10). This leads to an ordered region called a protodomain (analog to a nematic spherulite). Then the protodomains grow in size and eventually coalesce, but as they were not causally connected, the choices for the Higgs phases do not necessarily match. Singularities of the Higgs phase appear where the boundaries of protodomains finally meet, giving rise to line-like singularities called cosmic strings.

b. Statistical physics of a cosmic string network Kibble and Zurek remarked that these phase transitions involves two competing velocity scales: (1) the velocity v_f at which the field fluctuations propagate and (2) the velocity v_p at which the parameter ruling the phase transition (here, the temperature) varies. When

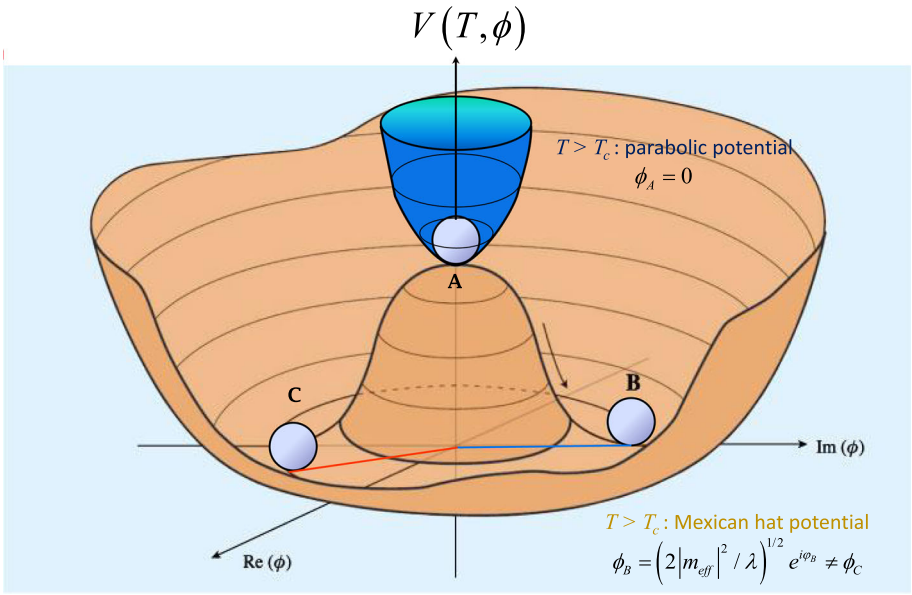

Fig. 10 A toy model from thermal field theory: the abelian Higgs model. At high temperatures, the parabolic potential gives a vanishing Higgs field ϕ, and the gauge symmetry is $U(1)$. At low temperatures, the parabolic potential gives a vanishing Higgs field ϕ, and the gauge symmetry is broken into I. Adapted from [119]

$v_p > v_f$, the system is quenched, and the parameters describing the resulting distribution of cosmic defects depend on the quench time τ_q in the form of scaling laws. For instance, the correlation length, the relaxation time, the average density of defects, and the variance of the net winding number σ are respectively given by

$$\xi(t) \sim \left|\frac{t-t_c}{\tau_q}\right|^{-\nu} \qquad \tau(t) \sim \left|\frac{t-t_c}{\tau_q}\right|^{-\mu} \qquad \rho(t) \sim \left(\frac{t}{\tau_q}\right)^{-\alpha} \qquad \sigma \sim N^{1/4} \tag{40}$$

where t_c is the time when the transition occurs [124], and N is the total number of defects in the region under investigation.

In the 1990s, several works [51, 52, 125–128] showed that the KZS, originally developed for cosmology, was also accurately describing disclinations in nematics with the very same scaling coefficients. For instance, this model predicts that the density of strings scales as $\rho \sim (t/\tau_q)^{\alpha}$ with a critical exponent $\alpha_{th} = 0.5$, and measurements performed by [51] with 5CB indeed gave $\alpha_{th} = 0.51 \pm 0.04$. The exponent characterizing the correlation between defects and antidefects is expected to be 1/4 and was measured at 0.26 ± 0.11 [125]. From the standpoint of statistical physics, phase transitions in cosmology and in liquid crystals seem to belong to the same universality class. But the family resemblance goes further. Networks of cosmic strings and networks of disclinations also share the same intersection processes: (1) when two line defects intertwine, they can reconnect the other way as they cross (intercommutation) [51, 129], and (2) when one line defect self-intersects, it generates a loop [130, 131].

c. Spacetime near a Nambu–Goto string The analogy between disclinations and cosmic strings goes even deeper. The simplest cosmic defects one may expect in the universe are called Nambu–Goto strings: they consist of delta-distributed concentrations of mass-energy and they can be pictured as infinitely straight and thin objects (the thickness of a realistic cosmic string is estimated at 10^{-28} cm). As required by thermal field theory and general relativity, the geometry around a Nambu–Goto string (in units where $c = 1$) is described by the Vilenkin's line element [129]:

$$ds^2 = -dt^2 + dr^2 + (1-4G\mu)^2 r^2 d\theta^2 + dz^2 \tag{41}$$

where μ is the string mass-energy density estimated at about 10 million billion tons per meter! The space part of this element is identical to (21), and it corresponds to a conical geometry with a removed Frank angle (typically, for a grand unified scale string, this angle is a few seconds of arc). As curvature is confined to the string axis, spacetime is locally flat away from the string, which exerts no gravitational pulling onto neighboring objects. Such object may of course generate a Berry phase in a similar fashion to their soft-matter cousin [132].

From the standpoint of the soft-matter physicist, Nambu–Goto strings can be understood as the cosmic counterparts of wedge disclinations. How to make sense of such incredible similarity? For the most part, this question is still open, but a noticeable attempt to address it was done in [133]. In essence, the reason is that equations of nematoelasticity have the form as the spatial sector of Einstein's field equations, with the elastic-stress tensor playing the role of the energy momentum tensor [75].

As the analogy between gravity and nematoelasticity does not concern time components, the dynamics of a cosmic defect cannot be directly mapped with those of a disclination. The motion of disclinations is classical (typically a few μm per second) and friction-dominated, whereas cosmic strings are ultra-relativistic, and dissipation mechanisms are due to radiation of gravitational waves. As noted in [51], this is intimately connected to

the nature of the broken symmetries: in particle physics, these latter are gauged (or internal), whereas in liquid crystals, broken symmetries are geometrical.[9]

4.3 Miscellanea

As a final bouquet, we will now discuss other fields in science where the key role played defects has been identified. Let us start with the wonder material of solid-state physics: graphene. This material was identified in 2004 by Geim and Novoselov, and since then, its amazing chemical and physical (electrical, mechanical, thermal) properties have propelled it to the scientific forefront. In fact, the perfect flatness of graphene plays a crucial role in its unusual behavior as local curvature modifies the local density of electronic states [134]. As graphene supports whole-integer disclination dipoles (pentagon–heptagon configurations known as Stone–Wales defects), one may expect to tailor the physical properties of graphene from distributions of topological defects: this is the emerging field of defect engineering. Tailoring graphene curvature with defects may even be relevant for medical sciences, as the curvature dependence of biomolecular adsorption may help discriminating between different molecules and removing harmful molecules in disease treatments [135]. Recently, tailoring transport in low-dimensional systems has been refined to the scale of quasi-particles, and immobile gauge modes known as fractons were shown to be intimately connected to disclinations [136].

Line defects also provide the answer to some fundamental questions in geology: as Earth's mantle is a solid layer made of rocks, how can it slip and move? Indeed, plasticity usually comes from the mobility of screw dislocations, but they are not sufficient to account for the rheology of the mantle. The main constituent of the upper mantle is olivine, at about 60–70%. In [137], it was shown that this layer was extremely rich in disclinations. Any applied shear on olivine-rich rocks induces grain-boundary migration mediated by disclination motions, explaining the motions of the Earth's mantle. This was confirmed by high-resolution electron backscattering diffraction.

Last but not least surprising is the central situation of line defects in high-energy physics. In [138], Deser, Jackiw, and 't Hooft proposed a model in 2+1 dimensions, where particles interacting gravitationally are described by a gas of conical defects, the mismatch angle being proportional to the particle's mass. This model was later extended to 3+1 dimensions by 't Hooft [139], but this time, matter particles are represented by a gas of piecewise straight string segments. An important feature of this model is that particles can have positive or negative masses, i.e., $\alpha < 1$ and $\alpha > 1$ Frank angles. This suggests that nematics could be used to perform high-energy physics experiments, in the spirit of the analog gravity game plan [140, 141]. The last word will be on quark physics. Topological insulators are currently garnering considerable attention because of their unusual electrical properties. The main difference between ordinary insulators and topological insulators (such as Chern, Kane-Mele) is the band inversion: spin–orbit couplings link valence and conduction bands. As a result of this connectivity, the surface states are topologically protected from local perturbations. Topological insulators may support disclinations in the bulk, which disrupt the lattice structure. This is responsible for the emergence of (quasi)particles of fractional charge, trapped at the defect location [142, 143]. This is likely to be of interest to simulate the elusive quarks, which have charge $-1/3e$ or $2/3e$.

5 Conclusion

Topological defects consist of regions of ordered systems where the order has broken down locally (for instance, after a phase transition), and as such they are among the most widespread structures in science. They carry generic topological and geometrical properties likely to impact a wide variety of physical processes, therefore enabling mutual cross-fertilization between different domains. For instance, the Kibble mechanism, initially designed for cosmology, was firstly tested with 5CB, a standard liquid crystal. Conversely, the existence of Mœbius defects in nematics suggests the search for more general cosmic defects in our universe (such as Alice strings which carry non-localized charges [144]).

Future prospects on topological defects look promising, both on the fundamental front and on the technological front. On the fundamental front, the search for cosmic strings is still in wait of a first robust observational evidence: so far, the NANOGrav collaboration have only reported stochastic gravitational-wave background signals compatible with, among others, networks of cosmic strings with a string parameter $G\mu$ in the range $\left[10^{-10.0}, 10^{-10.7}\right]$ [145]. Investigations on the role of defects in biology are still running at full tilt, and a recent review on open problems can be found in [146, 147]. One of the most challenging questions may be in understanding how the mechanical stresses due to defects couple to biochemical signaling.

Another booming field of research is the emerging field of defect engineering [148–150]. On the one hand, defects induce a change in the background geometry experienced by low-energy excitations. On the other hand, soft-matter systems, in particular liquid crystals, are indeed well-renowned contenders to build functionalized devices [151–153]. With advances in surface treatments, this has come to the point where it is now possible to prepare well-organized assemblies of topological defects from photo-patterning [154] or microwell structures [155] (see [149] for a review). Therefore, curvature/torsion can be taken advantage of to tailor the outgoing fluxes for applications in mechanical engineering (acoustics, electronics, thermotronics,

[9] Still, this difference is also the reason why we have used two different notations for vectors, $\mathbf{r}$ for the ordinary space vectors and $\vec{n}$ for the order parameter degrees of freedom.

optics; see e.g. [156–159]). Such perspectives are also under investigation in biology, where the possibility to control the dynamics of defects pairs was shown for tissues pre-patterned from photo-aligned liquid crystal elastomer [160]. Whatever the field of application, it leaves no doubt that taming topological defects is only at its first steps.

Acknowledgements This review is intended for students and researchers working in theoretical physics. It is written for the jubilee of Malte Henkel, our friend and colleague at Université de Lorraine, who has inspired many students during his career.

Data Availability Statement No data associated in the manuscript.

References

1. V. Poénaru, Elementary algebraic topology related to the theory of defects and textures. in *Ill-Condensed Matter: Les Houches Session XXXI*, (World Scientific, 1983), pp. 263–319
2. H. Kelker, History of liquid crystals. Mol. Cryst. Liq. Cryst. **21**(1–2), 1–48 (1973)
3. T. Sluckin, D. Dunmur, H. Stegemeyer, *Crystals that flow* (Taylor & Francis, London, 2004)
4. S.T. Lagerwall, On some important chapters in the history of liquid crystals. Liq. Cryst. **40**(12), 1698–1729 (2013)
5. D. Dunmur, T. Sluckin, *Soap, science, and flat-screen TVs: a history of liquid crystals* (Oxford University Press, Oxford, 2014)
6. M. Mitov, Liquid-crystal science from 1888 to 1922: Building a revolution. ChemPhysChem **15**(7), 1245–1250 (2014)
7. F. Reinitzer, Contributions to the knowledge of cholesterol. Liq. Cryst. **5**(1), 7–18 (1989)
8. O. Lehman, *Flüssige Kristalle sowie Plastizität von Kristallen im allgemeinen, molekulare Umlagerungen und Aggregatzustandsänderungen* (Verlag von Wilhelm Engelmann, Leipzig, 1904)
9. G. Friedel, Les états mésomorphes de la matière. In Annales de physique **9**, 273–474 (1922)
10. V.A. Belyakov, V.E. Dmitrienko, The blue phase of liquid crystals. Soviet Physics Uspekhi **28**(7), 535 (1985)
11. P. Oswald, P. Pieranski, *Nematic and cholesteric liquid crystals: concepts and physical properties illustrated by experiments* (CRC Press, New York, 2005)
12. P. Oswald, P. Pieranski, *Smectic and columnar liquid crystals: concepts and physical properties illustrated by experiments* (CRC Press, New York, 2005)
13. J.M. Kosterlitz, D.J. Thouless, Ordering, metastability and phase transitions in two-dimensional systems. J. Phys. C: Solid State Phys. **6**(7), 1181 (1973)
14. David R. Nelson. Defects and Geometry in Condensed Matter Physics. (2002)
15. D Frenkel. Liquids, freezing and glass transition. in *Les Houches Session*, pp. 689–762 (1991)
16. D. Andrienko, Introduction to liquid crystals. J. Mol. Liq. **267**, 520–541 (2018). (**Special Issue Dedicated to the Memory of Professor Y. Reznikov**)
17. P.-G. de Gennes, J. Prost, *The physics of liquid crystals*, vol. 83 (Oxford University Press, Oxford, 1993)
18. A.J. Leadbetter, R.M. Richardson, C.N. Colling, The structure of a number of nematogens. le Journal de Physique Colloques **36**(C1), C1–C37 (1975)
19. V. Tsvetkov, On molecular order in the anisotropic liquid phase. Acta Physicochim. URSS **16**, 132–147 (1942)
20. C.W. Oseen, The theory of liquid crystals. Trans. Faraday Soc. **29**(140), 883–899 (1933)
21. F.C. Frank, I. liquid crystals. on the theory of liquid crystals. Discuss. Faraday Soc. **25**, 19–28 (1958)
22. W. Maier, A. Saupe, Eine einfache molekulare theorie des nematischen kristallinflüssigen zustandes. Zeitschrift für Naturforschung A **13**(7), 564–566 (1958)
23. W. Maier, A. Saupe, A simple molecular statistical theory of the nematic crystalline-liquid phase. IZ Naturf. a **14**, 882–889 (1959)
24. S. Singh, *Liquid crystals: fundamentals* (World Scientific, Singapore, 2002)
25. G.R. Luckhurst, C. Zannoni, Why is the maier-saupe theory of nematic liquid crystals so successful? Nature **267**(5610), 412–414 (1977)
26. D. Feng, G. Jin, *Introduction To Condensed Matter Physics*, vol. 1 (World Scientific Publishing Company, Singapore, 2005)
27. P.G. De Gennes, Phenomenology of short-range-order effects in the isotropic phase of nematic materials. Phys. Lett. A **30**(8), 454–455 (1969)
28. P.G. De Gennes, Short range order effects in the isotropic phase of nematics and cholesterics. Mol. Cryst. Liq. Cryst. **12**(3), 193–214 (1971)
29. A.M. Sonnet, E.G. Virga, *Dissipative ordered fluids: theories for liquid crystals* (Springer, New York, 2012)
30. E.F. Gramsbergen, L. Longa, W.H. de Jeu, Landau theory of the nematic-isotropic phase transition. Phys. Rep. **135**(4), 195–257 (1986)
31. A. Majumdar, A. Zarnescu, Landau-de gennes theory of nematic liquid crystals: the oseen-frank limit and beyond. Arch. Ration. Mech. Anal. **196**(1), 227–280 (2010)
32. P.A. Lebwohl, G. Lasher, Nematic-liquid-crystal order–a monte carlo calculation. Phys. Rev. A **6**, 426–429 (1972)
33. S. Singh, Phase transitions in liquid crystals. Phys. Rep. **324**(2–4), 107–269 (2000)
34. G.R. Luckhurst, P. Simpson, Computer simulation studies of anisotropic systems: Viii. the lebwohl-lasher model of nematogens revisited. Mol. Phys. **47**(2), 251–265 (1982)
35. U. Fabbri, C. Zannoni, A monte carlo investigation of the lebwohl-lasher lattice model in the vicinity of its orientational phase transition. Mol. Phys. **58**(4), 763–788 (1986)
36. Z. Zhang, O.G. Mouritsen, M.J. Zuckermann, Weak first-order orientational transition in the lebwohl-lasher model for liquid crystals. Phys. Rev. Lett. **69**(19), 2803 (1992)

37. Z. Zhang, M.J. Zuckermann, O.G. Mouritsen, Phase transition and director fluctuations in the three-dimensional lebwohl-lasher model of liquid crystals. Mol. Phys. **80**(5), 1195–1221 (1993)
38. G. Skačej, C. Zannoni, The nematic-isotropic transition of the lebwohl-lasher model revisited. Phil. Trans. R. Soc. A **379**(2201), 20200117 (2021)
39. A. Gordillo-Guerrero, R. Kenna, J.J. Ruiz-Lorenzo, Scaling behavior of the heisenberg model in three dimensions. Phys. Rev. E **88**, 062117 (2013)
40. A.I.F. Sanchez, R. Paredes, B. Berche, Evidence for a topological transition in nematic-to-isotropic phase transition in two dimensions. Phys. Lett. A **308**(5), 461–466 (2003)
41. A.I. Fariñas-Sanchez, R. Botet, B. Berche, R. Paredes, On the critical behaviour of two-dimensional liquid crystals. Condens. Matter Phys. **13**(13601), 1–17 (2010)
42. Lander Burgelman, Lukas Devos, Bram Vanhecke, Frank Verstraete, Laurens Vanderstraeten. Contrasting pseudo-criticality in the classical two-dimensional heisenberg and RP^2 models: zero-temperature phase transition versus finite-temperature crossover, (2022)
43. B. Berche, A.I.F. Sanchez et al., Correlations in the low-temperature phase of the two-dimensional xy model. EPL (Europhysics Letters) **60**(4), 539 (2002)
44. C. Fan, M.J. Stephen, Isotropic-nematic phase transition in liquid crystals. Phys. Rev. Lett. **25**(8), 500 (1970)
45. W.M. Gelbart, B.A. Baron, Generalized van der waals theory of the isotropic–nematic phase transition. J. Chem. Phys. **66**(1), 207–213 (1977)
46. W.M. Gelbart, B. Barboy, A van der waals picture of the isotropic-nematic liquid crystal phase transition. Acc. Chem. Res. **13**(8), 290–296 (1980)
47. M.A. Anisimov, Universality of the critical dynamics and the nature of the nematic-isotropic phase transition. Mol. Cryst. Liq. Cryst. **146**(1), 435–461 (1987)
48. M.A. Anisimov, *Critical phenomena in liquids and liquid crystals* (CRC Press, New York, 1991)
49. S. handrasekhar, *Liquid crystals* (Cambridge University Press, Cambridge, 1992)
50. P.K. Mukherjee, The puzzle of the nematic-isotropic phase transition. J. Phys.: Condens. Matter **10**(41), 9191 (1998)
51. I. Chuang, R. Durrer, N. Turok, B. Yurke, Cosmology in the laboratory: Defect dynamics in liquid crystals. Science **251**(4999), 1336–1342 (1991)
52. M.J. Bowick, L. Chandar, E.A. Schiff, A.M. Srivastava, The cosmological kibble mechanism in the laboratory: string formation in liquid crystals. Science **263**(5149), 943–945 (1994)
53. M. Kleman, O.D. Lavrentovich, Topological point defects in nematic liquid crystals. Phil. Mag. **86**(25–26), 4117–4137 (2006)
54. B. Van Roie, J. Leys, K. Denolf, C. Glorieux, G. Pitsi, J. Thoen, Weakly first-order character of the nematic-isotropic phase transition in liquid crystals. Phys. Rev. E **72**(4), 041702 (2005)
55. G. Toulouse, M. Kléman, Principles of a classification of defects in ordered media. Journal de Physique Lettres **37**(6), 149–151 (1976)
56. M. Kléman, L. Michel, G. Toulouse, Classification of topologically stable defects in ordered media. Journal de Physique Lettres **38**(10), 195–197 (1977)
57. M. Kléman, L. Michel, Spontaneous breaking of euclidean invariance and classification of topologically stable defects and configurations of crystals and liquid crystals. Les rencontres physiciens-mathématiciens de Strasbourg-RCP25 **26**, 45–48 (1978)
58. N.D. Mermin, The topological theory of defects in ordered media. Rev. Mod. Phys. **51**(3), 591 (1979)
59. L. Michel, Symmetry defects and broken symmetry. Configurations hidden symmetry. Rev. Mod. Phys. **52**(3), 617 (1980)
60. G.E. Volovik, O.D. Lavrentovich, Topological dynamics of defects: boojums in nematic drops. Zh. Eksp. Teor. Fiz. **85**(6), 1997–2010 (1983)
61. M.V. Kurik, O.D. Lavrentovich, Defects in liquid crystals: homotopy theory and experimental studies. Soviet Physics Uspekhi **31**(3), 196 (1988)
62. M. Kléman, Defects in liquid crystals. Rep. Prog. Phys. **52**(5), 555 (1989)
63. Maurice Kleman. The topological classification of defects. Formation and Interactions of Topological Defects, 27–61 (1995)
64. G.E. Volovik, V.P. Mineev. Investigation of singularities in superfluid he 3 in liquid crystals by the homotopic topology methods. in *30 Years Of The Landau Institute–Selected Papers*, (World Scientific, 1996), pp. 120–130
65. R. Durrer, Topological defects in cosmology. New Astron. Rev. **43**(2–4), 111–156 (1999)
66. T.W.B. Kibble. Classification of topological defects and their relevance to cosmology and elsewhere. In itextitTopological defects and the non-equilibrium dynamics of symmetry breaking phase transitions, (Springer, 2000), pp. 7–31
67. Ç. Demiralp, J.F. Hughes, D.H. Laidlaw, Coloring 3d line fields using boy's real projective plane immersion. IEEE Trans. Visual Comput. Graphics **15**(6), 1457–1464 (2009)
68. F. Apéry, *Models of the real projective plane: computer graphics of Steiner and Boy surfaces* (Springer, New York, 2013)
69. G.P. Alexander, B.G. Chen, E.A. Matsumoto, R.D. Kamien, Colloquium: Disclination loops, point defects, and all that in nematic liquid crystals. Rev. Mod. Phys. **84**(2), 497 (2012)
70. B. Gin-ge Chen, P.J. Ackerman, G.P. Alexander, R.D. Kamien, I.I. Smalyukh, Generating the hopf fibration experimentally in nematic liquid crystals. Phys. Rev. Lett. **110**(23), 237801 (2013)
71. P.J. Ackerman, R.P. Trivedi, B. Senyuk, J. van de Lagemaat, I.I. Smalyukh, Two-dimensional skyrmions and other solitonic structures in confinement-frustrated chiral nematics. Phys. Rev. E **90**(1), 012505 (2014)
72. A.N. Bogdanov, U.K. Rößler, A.A. Shestakov, Skyrmions in nematic liquid crystals. Phys. Rev. E **67**(1), 016602 (2003)
73. J.-S.B. Tai, I.I. Smalyukh et al., Surface anchoring as a control parameter for stabilizing torons, skyrmions, twisted walls, fingers, and their hybrids in chiral nematics. Phys. Rev. E **101**(4), 042702 (2020)

74. A.I.F. Sánchez, R. Paredes, B. Berche, Topological transition in a two-dimensional model of liquid crystal. Phys. Rev. E **72**, 031711 (2005)
75. S.M. Carroll, *Spacetime and geometry* (Cambridge University Press, Cambridge, 2019)
76. C. Sátiro, F. Moraes, Lensing effects in a nematic liquid crystal with topological defects. Eur. Phys. J. E **20**(2), 173–178 (2006)
77. C. Sátiro, F. Moraes, On the deflection of light by topological defects in nematic liquid crystals. Eur. Phys. J. E **25**(4), 425–429 (2008)
78. E. Pereira, S. Fumeron, F. Moraes, Metric approach for sound propagation in nematic liquid crystals. Phys. Rev. E **87**(2), 022506 (2013)
79. S. Fumeron, F. Moraes, E. Pereira, Retrieving the saddle-splay elastic constant k24 of nematic liquid crystals from an algebraic approach. Eur. Phys. J. E **39**(9), 1–11 (2016)
80. A. De Padua, F. Parisio-Filho, F. Moraes, Geodesics around line defects in elastic solids. Phys. Lett. A **238**(2–3), 153–158 (1998)
81. A.M. de M Carvalho, C. Sátiro, F. Moraes, Aharonov-bohm–like effect for light propagating in nematics with disclinations. EPL (Europhysics Letters) **80**(4), 46002 (2007)
82. E. Cohen, H. Larocque, F. Bouchard, F. Nejadsattari, Y. Gefen, E. Karimi, Geometric phase from aharonov-bohm to pancharatnam-berry and beyond. Nat. Rev. Phys. **1**(7), 437–449 (2019)
83. P Richard. Feynman. statistical mechanics, a set of lectures. Frontiers in Physics. Perseus Books, (1972)
84. M.C. Marchetti, J.-F. Joanny, S. Ramaswamy, T.B. Liverpool, J. Prost, M. Rao, R.A. Simha, Hydrodynamics of soft active matter. Rev. Mod. Phys. **85**(3), 1143 (2013)
85. J.M. Yeomans, Nature's engines: active matter. Europhys. News **48**(2), 21–25 (2017)
86. Len Pismen. Active matter within and around us: From self-propelled particles to flocks and living forms. (2021)
87. M.R. Shaebani, A. Wysocki, R.G. Winkler, G. Gompper, H. Rieger, Computational models for active matter. Nat. Rev. Phys. **2**(4), 181–199 (2020)
88. George Gabriel Stokes et al. On the effect of the internal friction of fluids on the motion of pendulums. (1851)
89. P.A. Davidson, *Turbulence: an introduction for scientists and engineers* (Oxford University Press, Oxford, 2015)
90. There is also another set forming the Ericksen – Leslie equations, which are simpler but limited to uniaxial media and to smooth variations of the nematic ordering
91. A. Doostmohammadi, J. Ignés-Mullol, Julia M Yeomans, and Francesc Sagués. Active nematics. Nature communications **9**(1), 1–13 (2018)
92. D. Marenduzzo, E. Orlandini, J.M. Yeomans, Hydrodynamics and rheology of active liquid crystals: a numerical investigation. Phys. Rev. Lett. **98**(11), 118102 (2007)
93. S.P. Thampi, R. Golestanian, J.M. Yeomans, Vorticity, defects and correlations in active turbulence. Philos. Trans. R. Soc. A: Math. Phys. Eng. Sci. **372**(2029), 20130366 (2014)
94. L. Giomi, Geometry and topology of turbulence in active nematics. Phys. Rev. X **5**(3), 031003 (2015)
95. S.P. Thampi, J.M. Yeomans, Active turbulence in active nematics. Eur. Phys. J. Spec. Top. **225**(4), 651–662 (2016)
96. R. Alert, J.-F. Joanny, J. Casademunt, Universal scaling of active nematic turbulence. Nat. Phys. **16**(6), 682–688 (2020)
97. Amin, Doostmohammadi, Benoit, Ladoux. Physics of liquid crystals in cell biology. Trends in cell biology (2021)
98. C. Peng, T. Turiv, Y. Guo, Q.-H. Wei, O.D. Lavrentovich, Command of active matter by topological defects and patterns. Science **354**(6314), 882–885 (2016)
99. M.M. Genkin, A. Sokolov, O.D. Lavrentovich, I.S. Aranson, Topological defects in a living nematic ensnare swimming bacteria. Phys. Rev. X **7**(1), 011029 (2017)
100. Katherine Copenhagen, Ricard Alert, Ned S Wingreen, and Joshua W Shaevitz. Topological defects promote layer formation in myxococcus xanthus colonies. Nat. Phys. 17(2):211–215 (2021)
101. O.J. Meacock, A. Doostmohammadi, K.R. Foster, J.M. Yeomans, W.M. Durham, Bacteria solve the problem of crowding by moving slowly. Nat. Phys. **17**(2), 205–210 (2021)
102. V. Schaller, A.R. Bausch, Topological defects and density fluctuations in collectively moving systems. Proc. Natl. Acad. Sci. **110**(12), 4488–4493 (2013)
103. A. Chardac, L.A. Hoffmann, Y. Poupart, L. Giomi, D. Bartolo, Topology-driven ordering of flocking matter. Phys. Rev. X **11**(3), 031069 (2021)
104. M.-A. Fardin, B. Ladoux, Living proof of effective defects. Nat. Phys. **17**(2), 172–173 (2021)
105. P. Guillamat, C. Blanch-Mercader, G. Pernollet, K. Kruse, A. Roux, Integer topological defects organize stresses driving tissue morphogenesis. Nat. Mater. **21**(5), 588–597 (2022)
106. F.C. Keber, E. Loiseau, T. Sanchez, S.J. DeCamp, L. Giomi, M.J. Bowick, M.C. Marchetti, Z. Dogic, A.R. Bausch, Topology and dynamics of active nematic vesicles. Science **345**(6201), 1135–1139 (2014)
107. C. Blanch-Mercader, P. Guillamat, A. Roux, K. Kruse, Integer topological defects of cell monolayers: Mechanics and flows. Phys. Rev. E **103**(1), 012405 (2021)
108. Y. Maroudas-Sacks, L. Garion, L. Shani-Zerbib, A. Livshits, E. Braun, K. Keren, Topological defects in the nematic order of actin fibres as organization centres of hydra morphogenesis. Nat. Phys. **17**(2), 251–259 (2021)
109. F.D. Camargo, S. Gokhale, J.B. Johnnidis, D. Fu, G.W. Bell, R. Jaenisch, T.R. Brummelkamp, Yap1 increases organ size and expands undifferentiated progenitor cells. Curr. Biol. **17**(23), 2054–2060 (2007)
110. J.M. Lamar, P. Stern, H. Liu, J.W. Schindler, Z.-G. Jiang, R.O. Hynes, The hippo pathway target, yap, promotes metastasis through its tead-interaction domain. Proc. Natl. Acad. Sci. **109**(37), E2441–E2450 (2012)
111. J. Wang, L. Ma, W. Weng, Y. Qiao, Y. Zhang, J. He, H. Wang, W. Xiao, L. Li, Q. Chu et al., Mutual interaction

between yap and creb promotes tumorigenesis in liver cancer. Hepatology **58**(3), 1011–1020 (2013)
112. P. Marti, C. Stein, T. Blumer, Y. Abraham, M.T. Dill, M. Pikiolek, V. Orsini, G. Jurisic, P. Megel, Z. Makowska et al., Yap promotes proliferation, chemoresistance, and angiogenesis in human cholangiocarcinoma through tead transcription factors. Hepatology **62**(5), 1497–1510 (2015)
113. J.S.A. Warren, Y. Xiao, J.M. Lamar, Yap/taz activation as a target for treating metastatic cancer. Cancers **10**(4), 115 (2018)
114. J. Shen, B. Cao, Y. Wang, C. Ma, Z. Zeng, L. Liu, X. Li, D. Tao, J. Gong, D. Xie, Hippo component yap promotes focal adhesion and tumour aggressiveness via transcriptionally activating thbs1/fak signalling in breast cancer. J. Exp. Clin. Cancer Res. **37**(1), 1–17 (2018)
115. Y. Cheng, M. Mao, L. Yong, The biology of yap in programmed cell death. Biomark. Res. **10**(1), 1–10 (2022)
116. T.B. Saw, A. Doostmohammadi, V. Nier, L. Kocgozlu, S. Thampi, Y. Toyama, P. Marcq, C.T. Lim, J.M. Yeomans, B. Ladoux, Topological defects in epithelia govern cell death and extrusion. Nature **544**(7649), 212–216 (2017)
117. J. Zhang, N. Yang, P.K. Kreeger, J. Notbohm, Topological defects in the mesothelium suppress ovarian cancer cell clearance. APL Bioeng. **5**(3), 036103 (2021)
118. R. Jeannerot, J. Rocher, M. Sakellariadou, How generic is cosmic string formation in supersymmetric grand unified theories. Phys. Rev. D **68**(10), 103514 (2003)
119. J. Ellis, M.K. Gaillard, D.V. Nanopoulos, A historical profile of the higgs boson. The Standard Theory of Particle Physics: Essays to Celebrate CERN's 60th Anniversary, 255–274 (2016)
120. A.H. Guth, Inflationary universe: a possible solution to the horizon and flatness problems. Phys. Rev. D **23**(2), 347 (1981)
121. V. Mukhanov, *Physical Foundations of Cosmology* (Cambridge University Press, Oxford, 2005)
122. T.W.B. Kibble, Topology of cosmic domains and strings. J. Phys. A: Math. Gen. **9**(8), 1387 (1976)
123. W.H. Zurek, Cosmological experiments in condensed matter systems. Phys. Rep. **276**(4), 177–221 (1996)
124. P. Peter, J.-P. Uzan, *Primordial cosmology* (Oxford University Press, Oxford, 2009)
125. S. Digal, R. Ray, A.M. Srivastava, Observing correlated production of defects and antidefects in liquid crystals. Phys. Rev. Lett. **83**(24), 5030 (1999)
126. T. Kibble, Phase-transition dynamics in the lab and the universe. Phys. Today **60**(9), 47 (2007)
127. H. Mukai, P.R.G. Fernandes, B.F. De Oliveira, G.S. Dias, Defect-antidefect correlations in a lyotropic liquid crystal from a cosmological point of view. Phys. Rev. E **75**(6), 061704 (2007)
128. R. Repnik, A. Ranjkesh, V. Simonka, M. Ambrozic, Z. Bradac, S. Kralj, Symmetry breaking in nematic liquid crystals: analogy with cosmology and magnetism. J. Phys.: Condens. Matter **25**(40), 404201 (2013)
129. A. Vilenkin, Cosmic strings and domain walls. Phys. Rep. **121**(5), 263–315 (1985)
130. R.H. Brandenberger, Topological defects and structure formation. Int. J. Mod. Phys. A **9**(13), 2117–2189 (1994)
131. G. Duclos, R. Adkins, D. Banerjee, M.S.E. Peterson, M. Varghese, I. Kolvin, A. Baskaran, R.A. Pelcovits, T.R. Powers, A. Baskaran et al., Topological structure and dynamics of three-dimensional active nematics. Science **367**(6482), 1120–1124 (2020)
132. L.H. Ford, A. Vilenkin, A gravitational analogue of the aharonov-bohm effect. J. Phys. A: Math. Gen. **14**(9), 2353 (1981)
133. M. Simões, M. Pazetti, Liquid-crystals cosmology. EPL (Europhysics Letters) **92**(1), 14001 (2010)
134. A. Cortijo, M.A.H. Vozmediano, Effects of topological defects and local curvature on the electronic properties of planar graphene. Nucl. Phys. B **763**(3), 293–308 (2007)
135. B. Ni, T. Zhang, J. Li, X. Li, H. Gao, Topological design of graphene. Handb. Graph. **2**, 1–44 (2019)
136. M. Pretko, L. Radzihovsky, Fracton-elasticity duality. Phys. Rev. Lett. **120**(19), 195301 (2018)
137. P. Cordier, S. Demouchy, B. Beausir, V. Taupin, F. Barou, C. Fressengeas, Disclinations provide the missing mechanism for deforming olivine-rich rocks in the mantle. Nature **507**(7490), 51–56 (2014)
138. S. Deser, R. Jackiw, G. Hooft, Three-dimensional einstein gravity: dynamics of flat space. Ann. Phys. **152**(1), 220–235 (1984)
139. G. Hooft, A locally finite model for gravity. Found. Phys. **38**(8), 733–757 (2008)
140. C. Barceló, S. Liberati, M. Visser, Analogue gravity. Living Rev. Relat. **14**(1), 1–159 (2011)
141. M.J. Jacquet, S. Weinfurtner, F. König, The next generation of analogue gravity experiments (2020)
142. C. Ortix, Electrons broken into pieces at crystal defects (2021)
143. C.W. Peterson, T. Li, W. Jiang, T.L. Hughes, G. Bahl, Trapped fractional charges at bulk defects in topological insulators. Nature **589**(7842), 376–380 (2021)
144. M. Bucher, H.-K. Lo, J. Preskill, Topological approach to alice electrodynamics. Nucl. Phys. B **386**(1), 3–26 (1992)
145. J.J. Blanco-Pillado, K.D. Olum, J.M. Wachter, Comparison of cosmic string and superstring models to nanograv 12.5-year results. Phys. Rev. D **103**(10), 103512 (2021)
146. A. Ardaševa, A. Doostmohammadi, Topological defects in biological matter. Nat. Rev. Phys. **4**(6), 354–356 (2022)
147. Clarice D. Aiello, John M. Abendroth, Muneer Abbas, Andrei Afanasev, Shivang Agarwal, Amartya S. Banerjee, David N. Beratan, Jason N. Belling, Bertrand Berche, Antia Botana, Justin R. Caram, Giuseppe Luca Celardo, Gianaurelio Cuniberti, Aitzol Garcia-Etxarri, Arezoo Dianat, Ismael Diez-Perez, Yuqi Guo, Rafael Gutierrez, Carmen Herrmann, Joshua Hihath, Suneet Kale, Philip Kurian, Ying-Cheng Lai, Tianhan Liu, Alexander Lopez, Ernesto Medina, Vladimiro Mujica, Ron Naaman, Mohammadreza Noormandipour, Julio L. Palma, Yossi Paltiel, William Petuskey, João Carlos Ribeiro-Silva, Juan José Saenz, Elton J. G. Santos, Maria Solyanik-Gorgone, Volker J. Sorger, Dominik M. Stemer, Jesus M. Ugalde, Ana Valdes-Curiel, Solmar Varela, David H.

Waldeck, Michael R. Wasielewski, Paul S. Weiss, Helmut Zacharias, and Qing Hua Wang. A chirality-based quantum leap. *ACS Nano*, 16(4):4989–5035, 2022. PMID: 35318848
148. T. Araki, F. Serra, H. Tanaka, Defect science and engineering of liquid crystals under geometrical frustration. Soft Matter **9**(34), 8107–8120 (2013)
149. A. Jangizehi, F. Schmid, P. Besenius, K. Kremer, S. Seiffert, Defects and defect engineering in soft matter. Soft Matter **16**(48), 10809–10859 (2020)
150. M.J. Shin, D. Ki Yoon, Role of stimuli on liquid crystalline defects: From defect engineering to switchable functional materials. Materials **13**(23), 5466 (2020)
151. Paul J Ackerman, Zhiyuan Qi, Yiheng Lin, Christopher W Twombly, Mauricio J Laviada, Yves Lansac, and Ivan I Smalyukh. Laser-directed hierarchical assembly of liquid crystal defects and control of optical phase singularities. *Scientific reports*, 2(1):1–8, 2012
152. S. Fumeron, E. Pereira, F. Moraes, Principles of thermal design with nematic liquid crystals. Phys. Rev. E **89**(2), 020501 (2014)
153. W.K.P. Barros, E. Pereira, Concurrent guiding of light and heat by transformation optics and transformation thermodynamics via soft matter. Sci. Rep. **8**(1), 1–11 (2018)
154. Y. Guo, M. Jiang, S. Afghah, C. Peng, R.L.B. Selinger, O.D. Lavrentovich, Q.-H. Wei, Photopatterned designer disclination networks in nematic liquid crystals. Adv. Opt. Mater. **9**(16), 2100181 (2021)
155. H. Sakanoue, S. Yamashita, T. Murakami, H. Suzuki, K. Katayama, Controlled formation of topological defects of liquid crystals in micro-wells. Liq. Cryst. **49**(4), 580–588 (2022)
156. A. Manapany, L. Moueddene, B. Berche, S. Fumeron, Diffusion in the presence of a chiral topological defect. Eur. Phys. J. B **95**(7), 118 (2022)
157. S. Fumeron, B. Berche, E. Medina, F.A.N. Santos, F. Moraes, Using torsion to manipulate spin currents. EPL (Europhysics Letters) **117**(4), 47007 (2017)
158. E. Medina, L.A. González-Arraga, D. Finkelstein-Shapiro, B. Berche, V. Mujica, Continuum model for chiral induced spin selectivity in helical molecules. J. Chem. Phys. **142**(19), 194308 (2015)
159. Sébastien Fumeron, Bertrand Berche, and Fernando Moraes. Geometric theory of topological defects: methodological developments and new trends. in preparation
160. T. Turiv, J. Krieger, G. Babakhanova, H. Yu, S.V. Shiyanovskii, Q.-H. Wei, M.-H. Kim, O.D. Lavrentovich, Topology control of human fibroblast cells monolayer by liquid crystal elastomer. Sci. Adv. **6**(20), eaaz6485 (2020)
161. M. Nakahara, *Geometry, topology and physics* (IOP Publishing, Bristol, 2003)